NASA Technical Memorandum 4080

Investigation of a Moving-Model Technique for Measuring Ground Effects

Guy T. Kemmerly and John W. Paulson, Jr.
Langley Research Center
Hampton, Virginia

Summary

A ground-based testing technique is under development for the measurement of dynamic or time-dependent ground effects which may be present during aircraft approach and landing. The technique utilizes a model moving horizontally over an upwardly inclined ground plane to simulate rate of descent. This method contrasts with conventional wind-tunnel ground-effects testing techniques in which data are obtained at several fixed heights above the ground and is much more representative of actual flight conditions.

A relatively simple and comparatively inexpensive method of simulating rate of descent involves the use of the Langley Vortex Research Facility (VRF) to move a model horizontally over a ground plane consisting of an upwardly inclined ramp followed by a horizontal segment. The motion of the model over the ramp simulates an approach flight path angle, and the combination of the forward speed of the model and the ramp angle determines the simulated rate of descent.

Results were obtained in the VRF for both a generic 60° delta wing and an F-18 configuration, with and without thrust reversing, at forward speeds up to 100 ft/sec. The same models and support hardware were also tested in the Langley 14- by 22-Foot Subsonic Tunnel at identical conditions (but without rate of descent) with and without a moving-belt ground plane to obtain data for comparison.

Symbols

b	wing span, in.
C_D	coefficient of drag, $\frac{\text{Drag}}{qS}$
C_L	coefficient of lift, $\frac{\text{Lift}}{qS}$
ΔC_L	$C_{L,\text{instantaneous}} - C_{L,\text{reference}}$; in figures 14–30 subscript indicates the value of h/b used to obtain $C_{L,\text{reference}}$; $C_{L,\infty}$ indicates $C_{L,\text{reference}}$ was obtained at $h/b > 2.0$
C_m	coefficient of pitching moment, $\frac{\text{Pitching moment}}{qS(\text{MAC})}$
C_μ	ideal thrust coefficient, $\frac{\dot{m}V_j}{qS}$
h	height of model over ground board (referenced to MAC/4), in.
$\dot{h}$	rate of descent, ft/sec

$\dot{m}$	mass flow rate, slugs/sec
p	static pressure, psi
p_T	total pressure, psi
q	dynamic pressure, psf
S	wing area, ft^2
V	velocity, ft/sec
x	distance from leading edge of ground board, ft
α	angle of attack, deg
γ	flight path angle (incidence of model path relative to ground plane), deg
δ_f	flap deflection angle, deg
θ	incidence angle of model body axis referenced to ground plane, deg

Subscripts:

j	jet
∞	free stream

Abbreviations:

ips	inches per second
LaRC	Langley Research Center
MAC	mean aerodynamic chord
NPR	nozzle pressure ratio, $p_{T,j}/p_\infty$
sps	samples per second
VRF	Vortex Research Facility

Introduction

As fighter/attack aircraft designers continue to strive for increased aircraft performance and approach the limits of aerodynamic control, the tremendous power of the engine may soon be exploited to augment maneuverability through thrust vectoring. Once developed, this technology will almost certainly be used to improve takeoff and landing performance. With some enhancement, this capability may be useful in reducing the ground roll after landing by extending the vectored thrust technology into a thrust reverser. This is the premise on which the current investigation was performed. The objective was to develop a better understanding of the effects of vectored jets on the aerodynamics of aircraft in ground effect. This concern was addressed in reference 1 in the early stages of powered lift development. Measurements were made of the effect of a ground plane

1

on the lift coefficient of powered and unpowered models with and without a moving ground belt. The test program attempted to define a guide to be used in determining when it was necessary to perform ground effects testing over a moving ground plane. It was decided that, as a conservative approach, any test condition that indicated a ground effect on the lift coefficient required the moving-belt ground plane be used to improve the ground boundary-layer modeling in the test section. The results are summarized in the very simple plot shown in figure 1. In short, if the test conditions are such that

$$(h/b)/C_L < 0.05$$

a moving ground plane is required to simulate properly the ground boundary layer under an aircraft in ground effect. Otherwise, it is sufficient merely to remove the boundary layer at the leading edge of the test section.

This work was performed with high aspect ratio models, however, and may not be applicable when testing configurations with low aspect ratio wings and high wing loadings. This concern is illustrated in figure 2, which shows the longitudinal aerodynamic coefficients from a more recent ground effects study on a low aspect ratio jet flap configuration (ref. 2). The data are presented for the unpowered case; for a case with only half-span blowing (which is representative of a high aspect ratio vectored nozzle); and for a case in which the entire span of the flap was blown, representing a distributed jet. The unpowered case responds to the ground as would be expected in the classical sense (i.e., increased lift, slight drag reduction, and nose-down pitching moment), whereas the powered examples clearly begin to show ground effects at values of

$$(h/b)/C_L >> 0.05$$

In fact, powered lift ground effects can be seen to begin at values as high as

$$(h/b)/C_L = 0.15$$

This supports the concern that the work reported in reference 1 may not apply to the ground effects testing of advanced fighter configurations.

Other ground effects testing (refs. 3 and 4) suggests that there are certain transient elements associated with ground effects that are not properly modeled in typical wind-tunnel-based ground effects testing. In particular, conventional wind-tunnel ground effects tests (i.e., time-averaged tests of a stationary model at various ground heights) actually simulate

an aircraft flying near the ground at a particular altitude rather than an aircraft descending through that altitude as in an actual aircraft approach. Flight test results of a Concorde aircraft (ref. 5) showed that the ground effects measured during constant-altitude, low-level flights agreed very well with those predicted by wind-tunnel tests. On the other hand, it was found that the ground effects measured in the flight tests of the XB-70 aircraft (ref. 3) did not match those predicted in the static wind-tunnel tests of the configuration; the flight test results showed less lift increase during approach than was predicted on the basis of wind-tunnel testing. When rate of descent was simulated in the testing, however, a much better match with the flight test results was obtained. This is illustrated in figure 3 and reported in reference 4.

In the present investigation, the ground effects on two models were measured with and without rate-of-descent simulation. Figure 4 illustrates some of the important differences between conventional static ground effects test methods and the moving-model method. Static test techniques involve setting a model at a given height above the ground plane, allowing the flow field to reach a steady state, and measuring the aerodynamic loads. The moving-model technique, on the other hand, involves measuring the aerodynamics while the model is in motion and the flow field is in a dynamic state, similar to conditions in an actual approach. Simulations of normal approaches (without thrust reversers) have indicated only small, but discernible, differences in model aerodynamics measured statically and at various rates of descent, as shown in figure 5. With thrust reversers or similar jet devices operating, however, the two techniques could yield significantly different results. There are two primary reasons for the expected differences. The first is the time-dependent (unsteady) aerodynamic effects related to the motion of the model and the developing jet exhaust plume. The other difference is due to the different model attitudes (relative to the ground plane) required to set a particular angle of attack. The vertical component of velocity inherent in the moving-model technique reduces the incidence angle of the model, θ (in comparison with the static test technique), necessary to achieve a given angle of attack. This reduced incidence angle changes both the impingement angle and the impingement point of the jet on the ground plane, resulting in distinctly different plumes in the two test techniques.

Based on the investigations and observations in references 1–5, and in view of the known sensitivity of powered configurations to ground boundary-layer modeling, it appeared that conventional

ground-effects testing techniques should be reevaluated. The main emphasis in the present investigation was to determine the effects of rate of descent by comparing the results of current static testing methods with results from a dynamic procedure in which a model would be moved toward an inclined ground plane to simulate rate of descent. A second objective of the study was to evaluate the need for using a moving-belt ground plane when testing configurations with thrust reversers in wind tunnels. The parameter studied in this investigation was lift coefficient. This paper presents the details of the dynamic testing technique and provides an assessment of the effects of both the moving-belt ground plane and the moving model as they influence the development of aerodynamic ground effects.

Throughout this paper, the term "static" refers to results obtained in the 14- by 22-Foot Subsonic Tunnel with a stationary model; "dynamic" refers to results obtained in the VRF while the model was moving over the inclined portion of the ground board to simulate rate of descent; and "steady state" refers to the results obtained in the VRF while the model was moving at a fixed height over the level portion of the ground board.

Models

The first model tested was a 36-in-span, 60° delta wing made from 3/8-in. clear acrylic sheet. The leading and trailing edges were beveled to sharp edges with a 7.5° half angle. A sketch of the model is shown in figure 6. The model was supported by a six-component strain-gauge balance mounted on the centerline of the model, 6 in. forward of the trailing edge. Two nonmetric axisymmetric jets were used to simulate reverse thrust and were mounted at the trailing edge to exhaust foward at a 45° angle. The nozzle exits were 1 in. below the trailing edge of the wing and were spaced 4 in. apart. Simple convergent nozzles were used and are detailed in figure 7.

The other model used in the study was a 0.07-scale F-18 model shown in figures 8 and 9. The model was mounted on a six-component strain-gauge balance inside the fuselage, and it was equipped with adjustable leading- and trailing-edge flaps and horizontal stabilizer. Reverse thrust simulation was supplied nonmetrically with a thrust reverser simulator described in reference 6 and sketched in figure 10. The simulator provided for variability in both longitudinal reverser angle and splay angle (the angle that the jets are inclined spanwise). The jet was directed by honeycomb inserts embedded in the plenum box cover plate. Different plates directed the jets at different angles.

Test Facilities and Procedures

The same models, support systems, and air lines were tested first in the Langley Vortex Research Facility (VRF) and then in the Langley 14- by 22-Foot Subsonic Tunnel. The models were tested at several rates of descent, forward speeds, and thrust reverser settings.

The Vortex Research Facility (fig. 11) at the Langley Research Center was modified for the present study by installing a 150-ft-long ground plane assembly approximately in the center of the test section. The models were suspended on a variable-length strut extending from the bottom of the gasoline-engine-powered cart. The strut supported the model, sting, and air line assembly as well as the instrumentation. It also provided a means for adjusting the minimum height over the level portion of the ground board. Angle of attack was changed by pitching the entire strut, sting, and model assembly at the point where the strut was attached to the cart. Velocity was controlled by a cruise control system on the cart. High-pressure air bottles on the cart provided compressed air for the jets. The ground board consisted of two parts: a ramp that was inclined upward 4° for a distance of 100 ft, followed by a horizontal section that extended for an additional 50 ft. As the model moved horizontally over the inclined portion, the height of the model above the ground board decreased, thereby simulating an approach along a glide slope of 4°. Rate of descent was dependent on the test velocity as given by the equation

$$\dot{h} = V_\infty \tan 4°$$

After moving across the ramp, the model passed over the horizontal section to simulate rollout or constant altitude flight. (See fig. 12.) In the VRF, 24 channels of data are transmitted from the cart through a modulated laser to a photoreceptor and a mass storage unit. The channels are sampled at a rate of 111 sps for nearly 30 sec. The data are then converted to engineering units using a Hewlett-Packard HP 1000 A900 computer. For more information on the data acquisition in the VRF see reference 7.

The static ground effects of the models were measured in the Langley 14- by 22-Foot Subsonic Tunnel, which has a suction ground boundary-layer removal system and a relatively large test section, as illustrated in figure 13. The boundary-layer removal system is located at the beginning of the test section and is followed by a moving-belt ground plane which is used to minimize boundary-layer development in the test section. The models were supported from the aft bay of the test section and extended into the front bay over the moving-belt ground plane. Angle

3

of attack was controlled by pitching the sting and the vertical strut, and height was changed by driving the entire support system vertically. Angle of attack was measured by an accelerometer installed on the model, and height was computed from readings obtained by encoders on the support system. The data in the 14- by 22-Foot Subsonic Tunnel are time-averaged over a period of 4 sec for each data point. The sample rate is 5 sps, resulting in 20-sample averages. Data acquisition processing is controlled through the ModComp Classic 7863 computer system in the facility.

Instrumentation and Error

Forces and moments were measured with a six-component strain gauge balance (NASA LaRC FF09). For the component used in this investigation, the error range on each model was as follows:

$$C_L = \pm 0.0027$$

for the delta wing model, and

$$C_L = \pm 0.0033$$

for the F-18 model. These ranges are based on the results of a special calibration of the balance, which showed a normal force error of ± 0.1 percent of the full-scale calibrated load of 100 lb. The axial force error used was that typically quoted for NASA balances, ± 0.5 percent of full scale.

Jet total temperatures were measured in iron-constantan thermocouples located approximately 6.5 ft upstream of the nozzle exits. Iron-constantan thermocouples have a possible error, based on the manufacturer's specifications, of $\pm 1.1°C$, which converts to $\pm 1.98°R$. In addition, a calibration of the wire and sensing unit indicated an error of $\pm 0.6°R$, giving a total system error of $\pm 2.58°R$.

Jet exit total pressures were statically calibrated against total pressure measurements taken at a point approximately 2.33 ft upstream of the nozzle exits by using two CEC Model 4-312 pressure transducers, each having a total range of 100 psi. During these calibrations, nozzle exit pressures were measured on a ± 20 psid Mensor pressure transducer. After calibration relationships were established, the total-pressure probes were removed from the nozzles and exit total pressures were computed from the upstream measurements. The error on the CEC transducers is ± 0.75 percent of the full-scale range, according to the manufacturer, or ± 0.75 psi. The Mensor pressure transducer has an accuracy of ± 0.04 percent of full scale or ± 0.008 psi.

Sting accelerations were measured using Setra Systems $\pm 15g$ linear accelerometers calibrated over a range of $\pm 1g$. In the test section, during the cruise portion of the runs, $\pm 1g$ was sufficient to encompass the accelerations of the vibrating model. The Setra Systems accelerometers have a manufacturer's specified accuracy of ± 1 percent of full scale; however, the results of an in-house calibration of the accelerometers indicate they have an accuracy of ± 0.1 percent of full scale over the range of $\pm 1g$, or $\pm 0.001g$. Cart accelerations were not used in data analysis. The details of how these accelerations were used to remove the inertial loads from the balance data are given in appendix A.

Velocity was measured at one point in the test section by using a laser beam shining across the path of the vehicle. A 1-ft-long plate on the nose of the vehicle cut the beam as the cart passed the laser position; the time that the beam was interrupted was used to compute the velocity of the vehicle at that point. This was correlated to the rotation rate of a wheel on the cart as it passed that point in the test section. This correlation was then used to compute vehicle speed from wheel rotation rate for all other points in the run. Integration of the velocity channel over the entire length of the test section for all runs indicated a total system error of the integrated velocity measurement of ± 5 ft in 500 ft, or ± 1 percent in the velocity measurement.

To determine the position of the model in the facility at each point, the velocity channel was integrated forward and aft from one known location in the middle of the test section. This procedure is detailed in appendix B.

Relative humidity and temperature were measured with a General Eastern Instruments Model 400E relative humidity and temperature indicator. Humidity was measured with a sulfonated polystyrene resistance grid having an accuracy of ± 3 percent and a hysteresis of ± 3 percent, according to the manufacturer's specifications. The temperature sensor was a ceramic-enclosed platinum resistance element used in a three-wire resistance temperature device having an accuracy of $\pm 1°R$.

Results

Because of the exploratory nature of this first entry into the VRF, limited run matrices were executed with each model. Tables I and II define the conditions tested.

Ground proximity has a measurable effect on many aspects of the performance of a configuration. In this investigation the criterion used in monitoring ground effects was the change in lift coefficient. As

a result, all data are plotted as the change in lift coefficient versus ground height.

60° Delta Wing

The results of tests on the 60° delta wing are presented in figures 14–21 in terms of the change in lift coefficient due to ground proximity relative to the lift coefficient measured at the highest model height common to all three test techniques. Each figure shows the ground effects measured on the moving model at one rate of descent and those measured in the wind tunnel over both the fixed and the moving ground plane. The moving-model results for the delta wing were obtained at a nominal sink rate of 6.3 ft/sec.

For the power-off case at low angle of attack (fig. 14) there are virtually no differences in measured ground effects between the different test techniques. However, when the thrust reversers were operated (fig. 15) the results were quite different. At NPR = 1.8 the static data indicate maximum lift occurred at about $h/b = 0.75$ when testing without the moving-belt ground plane. Eliminating the ground boundary layer by using the moving-belt ground plane delayed this peak until $h/b = 0.6$. In sharp contrast to the static test data, the moving-model data from the VRF indicate that lift continued to increase down to the minimum ground height of $h/b = 0.25$ and not until the model was over the horizontal portion of the ground board for some time did lift begin to decrease. It is not known why the steady state results from the VRF do not match the static data obtained in the wind tunnel over the moving-belt ground plane.

Increasing thrust to NPR = 2.0 showed no further differences in the data trends, as can be seen in figure 16. There was a net loss in lift for the VRF steady state results at $h/b = 0.25$ for this power setting, indicating that "suckdown" effect is greater than for NPR = 1.8, as would be expected.

The power-off data obtained at an angle of attack of 10° are shown in figure 17 and are relatively consistent among the three test procedures. The effect of power shown in figures 18 and 19 is essentially the same as was measured for $\alpha = 1.5°$.

The moving-model results show that there was a large delay in the onset of lift loss measured in the VRF relative to the wind-tunnel results. This is primarily due to the differences in the thrust reverser flow fields generated by the two techniques (illustrated in fig. 4). This characteristic will be seen to persist to some degree in all subsequent data.

For $\alpha = 14°$, the static ground effects measured in the wind tunnel with power off became evident at a relatively large h/b, greater than 1.0, with or without the moving-belt ground plane in operation (fig. 20).

In the VRF, however, the power-off ground effects measured with the moving-model technique did not become apparent until a much lower h/b of about 0.5 had been reached. The steady state VRF data obtained over the horizontal portion of the ground board, however, did correlate well with the static wind-tunnel data. Similar results were obtained in the study reported in reference 5, which shows good correlation between wind-tunnel data and constant altitude flyover tests of a non-thrust reversing delta wing aircraft. The effect of ground proximity at NPR = 2.0 (fig. 21) was similar to the effects observed at lower angles of attack but was more pronounced. The steady state lift loss was much less than was observed in the wind tunnel, and the dynamic ground effects resulted in a lift increase down to $h/b = 0.42$.

F-18

For the F-18 model, a nominal sink rate of 7.0 ft/sec was used. It is also important to note that many times it was not possible to test in the wind tunnel at great heights because of support system limitations. For these cases the increments in lift coefficient have been referenced to the values at the maximum height for which data were obtained by all three techniques. Note also that the moving-model data were obtained at a lower minimum ground height than the wind-tunnel data; however, the steady-state VRF data usually correlate well with the lift loss that would be expected to occur in the wind-tunnel results were they extrapolated to the lower height.

The results from the 0.07-scale F-18 show trends similar to those observed for the 60° delta wing model test. However, the ground effect on the F-18 was smaller and less sensitive to rate of descent. This is attributed, primarily, to two basic differences in the configurations. Because the thrust reversers were located well behind the wing on the F-18 in comparison with the delta wing, their influence on ground effects was less. (Note the difference in scale between the delta wing data and the F-18 data.) The higher aspect ratio wing of the F-18 also reduces its sensitivity to rate-of-descent modeling, as discussed in reference 4. These smaller increments in the aerodynamic coefficients make the quoted balance inaccuracies significant in the F-18 results; however, because of the consistency of the data trends, the following conclusions drawn from the data are considered to be valid

Throughout the discussion of the F-18 results, the term "clean configuration" refers to the model condition in which the leading- and trailing-edge flaps, as well as the horizontal stabilizer, were undeflected. The term "high-lift configuration" describes the

situation in which the leading-edge flaps were deflected 25°, the trailing-edge flaps were deflected 20°, and the horizontal stabilizer was deflected −10°. The rudders were not deflected for any of the runs.

As shown in figure 22, all three techniques indicated negligible ground effects at $\alpha = 1.5°$ when the thrust reversers were not operating. However, at NPR = 1.45 (fig. 23) and 1.95 (fig. 24), the onset of lift loss occurred at lower ground heights for the moving-model VRF technique than for the wind-tunnel techniques.

As noted previously, the thrust reverser simulator used with the F-18 incorporates provision for varying the splay angle of the reverser jets. Figure 25 presents the data for the reverser jets deflected 40° outward toward the wingtips. When these data are compared with figure 23, it is apparent that blowing spanwise avoids the severe lift loss experienced when blowing forward parallel to the model centerline. This result has been noted before in thrust reverser testing and is explained in reference 8. Also note that the steady state data taken with the moving model seem to be in general agreement with an extrapolation of the wind tunnel to $h/b = 0.18$. This was an expected result because the steady state VRF data and the wind-tunnel data taken over the moving-belt ground plane are both measurements taken with no rate of descent and no ground boundary layer. As stated earlier, it is not understood why these data did not correlate better in the delta wing test.

Data obtained with the leading- and trailing-edge flaps deflected are illustrated in figures 26–28. With the model unpowered and at a low angle of attack, all three techniques produced very similar ground effects, as can be seen in figure 26. At NPR = 2.0 (fig. 27) the ground effect trends were similar to the previously discussed case with undeflected flaps. That is, lift loss associated with close ground proximity was delayed with the moving model as compared with the conventional tests. When thrust reverser power was increased to NPR = 2.5, the moving-belt wind-tunnel data are in fairly good agreement with VRF results, as seen in figure 28. This would indicate that the time-dependent effect is a function of the time necessary for the plume to develop in front of the model. High-powered jets penetrate further and stagnate on the floor at higher ground heights than low-powered jets. Once the jet stagnates it will separate into a forward-moving wall jet and an aft-moving wall jet. The forward-moving wall jet then develops into the plume that affects the model aerodynamics. Very high-powered jets can penetrate the flow field better and begin the formation of the plume

sooner, perhaps masking the effect of sink rate. This suggests that there is an upper bound to the need for this type of testing. In the limit, an aircraft that lands at a very low rate of descent and high power setting (such as a Harrier or any other vertical landing aircraft) would probably not benefit much from modeling the rate of descent.

At $\alpha = 8.4°$ and NPR = 1.5, the data of figure 29 show the typical delayed suckdown in the VRF as compared with static wind-tunnel results. On the other hand, results at NPR = 2.5 (fig. 30) show good agreement among all three techniques in the value of h/b for maximum lift increase, as was noted earlier at a high power setting. It should be noted, however, that the level of maximum lift increments were not well matched between the wind-tunnel and VRF data.

Concluding Remarks

The moving-model technique shows significantly different ground effects than those measured from conventional wind-tunnel ground effects testing. It was found that the F-18 was considerably less sensitive to rate-of-descent modeling than was the delta wing, indicating that the effects of that parameter are strongly configuration dependent. The implications of the results obtained appear to be especially significant for short takeoff and landing configurations with thrust reversers. Moving models having no thrust simulation showed small, but different, levels of ground effects than those measured by conventional static wind-tunnel tests. On the other hand, models with thrust reversers exhibit dramatically different trends in the aerodynamics associated with ground effects. The data also show that, while the use of a moving-belt ground plane can improve the correlation of static ground effects data somewhat, the results are still considerably different from those measured on a moving model.

In this limited exploratory investigation the problem of scaling the results of the dynamic test technique to full scale was not addressed. However, for this method to be useful in obtaining aerodynamic design data, that problem must eventually be addressed. As a first step in doing so, a further study should investigate the effect of varying rate of descent and jet velocity over a wider range and correlate the results with a flight test program.

NASA Langley Research Center
Hampton, VA 23665-5225
December 6, 1988

Appendix A

Special Corrections

An inherent problem with moving-model testing is that model motion caused by vibrations of the cart and strut will contaminate the balance aerodynamic force data with inertial loads and loads due to aerodynamic damping. These loads must be removed from the balance output in order to identify the aerodynamic data contained in the balance output. The strut and cart were therefore instrumented with several accelerometers to measure the vertical and lateral accelerations of the sting and the vertical, lateral, and longitudinal accelerations of the cart near the strut connection point. The velocities necessary to compute the damping loads were computed by integrating the accelerometer outputs. Early analysis of the data showned the damping terms to be considerably smaller than the inertial terms and extremely difficult to estimate, so they were not removed from the data. Evidence also indicates (refs. 9 and 10) that the lift on oscillating airfoils cannot be accurately predicted based only on angle of attack and a static lift curve slope, making the calculation of instantaneous lift loads even more complicated.

As a first-order approximation of the inertial loads, the total mass of the model and all mounting hardware on the model side of the balance strain gauges was multiplied by the measured vertical acceleration of the sting. The resulting loads were then subtracted from the normal force outputs of the balance to obtain the aerodynamic normal force acting on the model.

According to reference 11, it was necessary to filter the data before digitizing it in order to avoid contamination of the sampled data with unwanted higher frequencies. This contamination is referred to as aliasing. The data, sampled at roughly 111 sps, therefore required filtering to at least 50 Hz. The highest frequency filters available for this system were 10 Hz filters, so the data were obtained containing frequencies up to 10 Hz. When looking for time-dependent effects, it is desirable to have the data as unfiltered as possible to avoid phase shifting or smoothing over the rapid aerodynamic effects associated with phenomena such as separation and suckdown. Therefore, beyond the necessary filtering to 10 Hz and the removal of the inertial loads, the data were faired by hand. An example of this process is illustrated in figure 31.

Appendix B

Cart Position Calibration

In previous tests in the VRF, it was not critical that the cart position be precisely known. When a ground board was installed in the VRF, however, this became necessary because h/b is a function of cart position. Previously, the system had a maximum error of 1 ft. That converts to an h/b error of 0.023 (for a 3-ft-span model) over the inclined portion of the ground board. This was determined to be unacceptable for these tests.

To minimize this error, a linearly increasing voltage source was installed on the vehicle and was monitored through one of the data channels. When the vehicle passed a known position in the test section, the voltage source was triggered and began to increase linearly from a starting level of zero volts. The rate of increase was such that the level would not achieve its full-scale value of 10 V in less than 0.00899 sec, the period of time between data samples at the VRF. The first nonzero reading on that channel, therefore, indicated precisely how long after the vehicle had passed the trigger that the channel was sampled. By knowing the exact trigger position, the position of the vehicle could then be calculated precisely for one point in the middle of the test section. Forward and backward integration from that point of the velocity channel gave all other positions.

To calibrate the device and ensure that it increased linearly, its input (trigger signal) and outputs were recorded on an FM tape recorder (operating at 15 ips) and played back onto an oscillograph recorder. By monitoring the trigger signal it was shown that, statically, the device had no detectable time delay between triggering and the onset of output rise. It was found that the output was very linear and increased at a rate of 932.7 V/sec over the first 0.00899 sec. Therefore, it would not reach the full scale 10 V in less than 0.00899 sec.

Once the voltage ramp system was installed in the vehicle, another element of the system was calibrated. This calibration was to determine the delay time, at actual testing velocities, between the vehicle passing the trigger location and the trigger signal actually reaching the voltage ramp device. A photocell was placed on the vehicle such that it would be illuminated by a laser the moment the cart reached the trigger location in the test section. Monitoring the output of the photocell and the input to the voltage ramp device on an FM tape recorder (operating at 15 ips) showed a time delay of 0.0050 sec to be in the system because of the action of the switch. This was taken into account when computing vehicle position. It should also be noted that the reaction time of the photocell was on the order of 10^{-9} sec (according to the manufacturer's specifications) and was therefore considered to be instantaneous.

References

1. Turner, Thomas R.: *Ground Influence on a Model Airfoil With a Jet-Augmented Flap as Determined by Two Techniques.* NASA TN D-658, 1961.

2. Stewart, V. R.: *Low Speed Wind Tunnel Test of a Propulsive Wing/Canard Concept in the STOL Configuration. Volume II: Test Data.* NASA CR-178349, 1987.

3. Baker, Paul A.; Schweikhard, William G.; and Young, William R.: *Flight Evaluation of Ground Effect on Several Low-Aspect-Ratio Airplanes.* NASA TN D-6053, 1970.

4. Chang, Ray Chung: *An Experimental Investigation of Dynamic Ground Effect.* Ph.D. Diss., Univ. of Kansas, 1985.

5. Pelagatti, C.; Pilon, J. C.; and Bardaud, J.: Analyse Critique des Comparaisons des Resultats de Vol aux Previsions de Soufflerie Pour des Avions de Transport Subsonique et Supersonique. *Flight/Ground Testing Facilities Correlation,* AGARD-CP-187, Apr. 1976, pp. 23-1–23-24.

6. Joshi, P. B.; Widynski, T. C.; Chiarelli, C.; and Chapman, R. W.: *Generic Thrust Reverser Technology for Near Term Application. Volume 2. Testing, Method Application and Data Analysis.* AFWAL-TR-84-3094-VOL. 2, U.S. Air Force, Feb. 1985. (Available from DTIC as AD B094 293L.)

7. Satran, Dale R.; Neuhart, Dan; Holbrook, G. Thomas; and Greene, George C.: Vortex Research Facility Improvements and Preliminary Density Stratification Effects on Vortex Wakes. AIAA-85-0050, Jan. 1985.

8. Gatlin, Gregory M.; Banks, Daniel W.; and Paulson, John W., Jr.: *Low-Speed Longitudinal Aerodynamics and Directional-Control Effectiveness of an Advanced Fighter Configuration With Multifunction Nozzles.* NASA TP-2794, 1988.

9. Atta, R.; and Rockwell, D.: Hysteresis of Vortex Development and Breakdown on an Oscillating Delta Wing. *AIAA J.,* vol. 25, no. 11, Nov. 1987, pp. 1512–1513.

10. Carr, Lawrence W.: Progress in Analysis and Prediction of Dynamic Stall. *J. Aircr.,* vol. 25, no. 1, Jan. 1988, pp. 6–17.

11. Hamming, R. W.: *Digital Filters,* Second ed. Prentice-Hall, Inc., c.1983.

Table I. Test Conditions for the 60° Delta Wing Model

α, deg	NPR	Figure
1.5	1.0	14
1.5	1.8	15
1.5	2.0	16
10.0	1.0	17
10.0	1.6	18
10.0	2.0	19
14.0	1.0	20
14.0	2.0	21

Table II. Test Conditions for the F-18 Model

α, deg	NPR	Splay, deg	Configuration	Figure
1.5	1.0	0	Clean	22
1.5	1.45	0	Clean	23
1.5	1.95	0	Clean	24
1.5	1.5	40	Clean	25
1.5	1.0	0	High lift	26
1.5	2.0	0	High lift	27
1.5	2.5	0	High lift	28
8.4	1.5	0	High lift	29
8.4	2.5	0	High lift	30
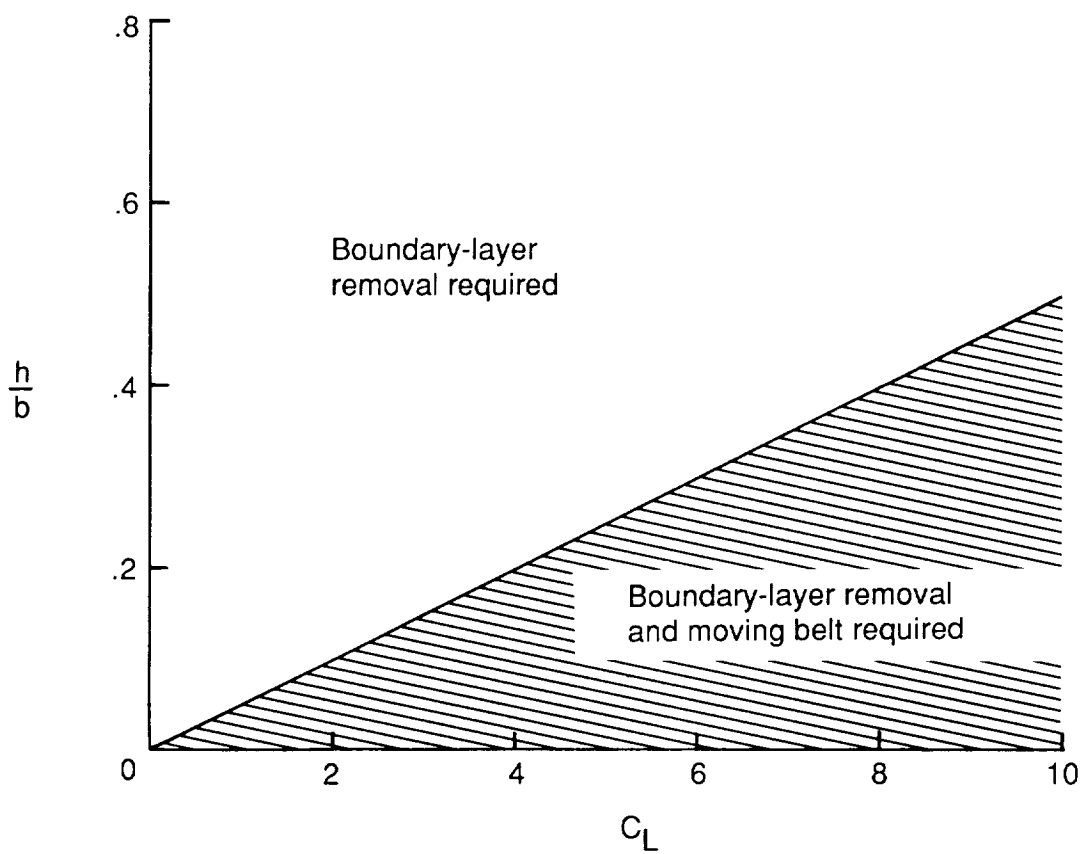
Figure 1. Criteria established in reference 1 for determining the need for a moving-belt ground plane.
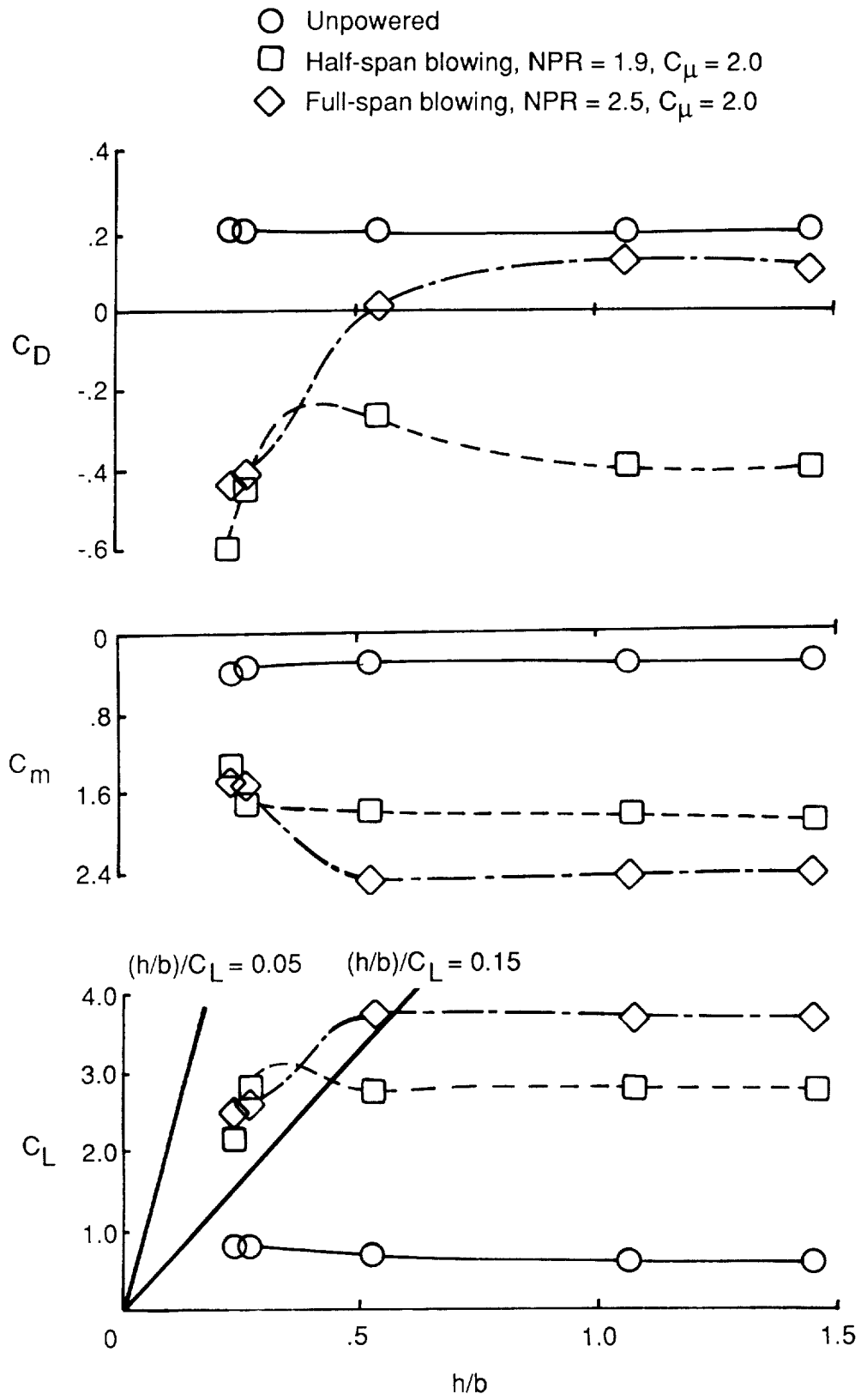
Figure 2. Ground effect on the longitudinal aerodynamics of a powered-lift configuration. $\alpha = 0°, \delta_f = 45°$.
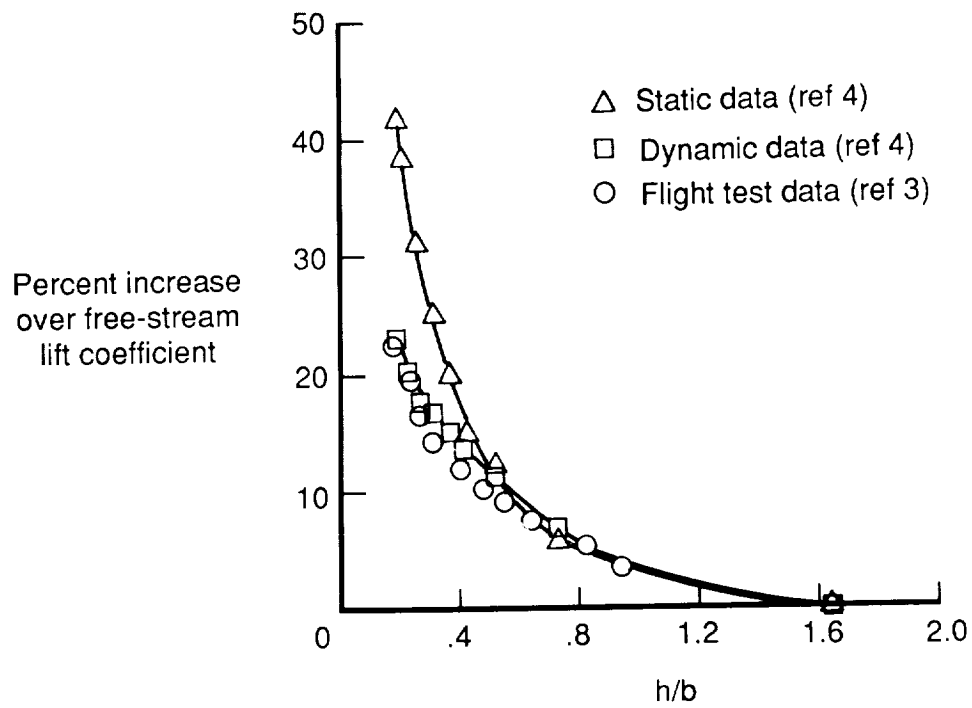
Figure 3. Static, dynamic, and flight test data from an XB-70 at $\alpha = 9.3°$.

Steady state
$\alpha = 12°$
$\gamma = 0°$
$\theta = 12°$
$\dot{h} = 0$ ft/sec

$\alpha = \theta$

V_∞

Dynamic
$\alpha = 12°$
$\gamma = -5°$
$\theta = 7°$
$\dot{h} = V_\infty \tan \gamma$

α

θ

γ

V_∞
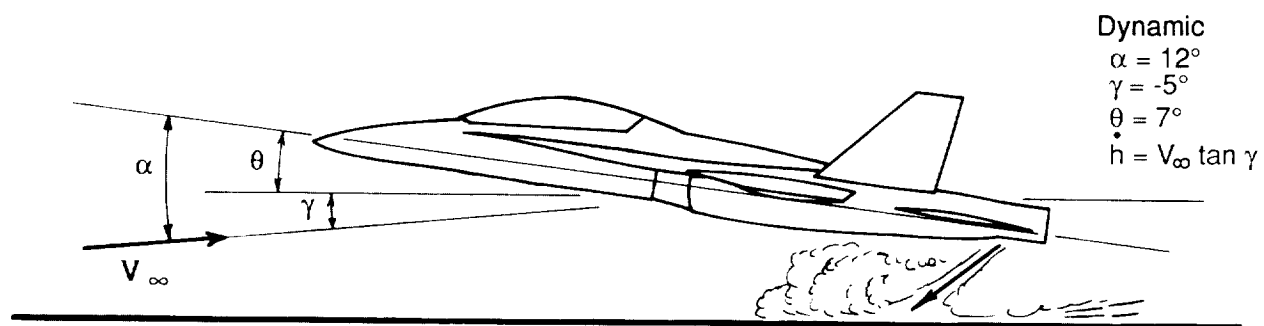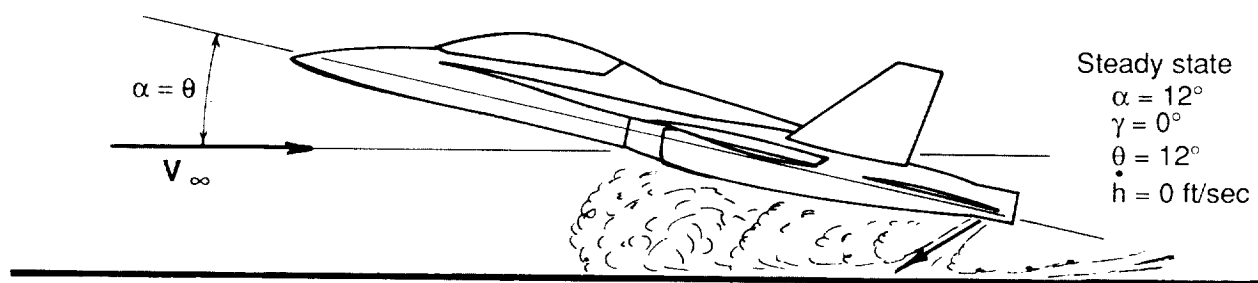
Figure 4. Schematic of dynamic and steady state ground effects.

14
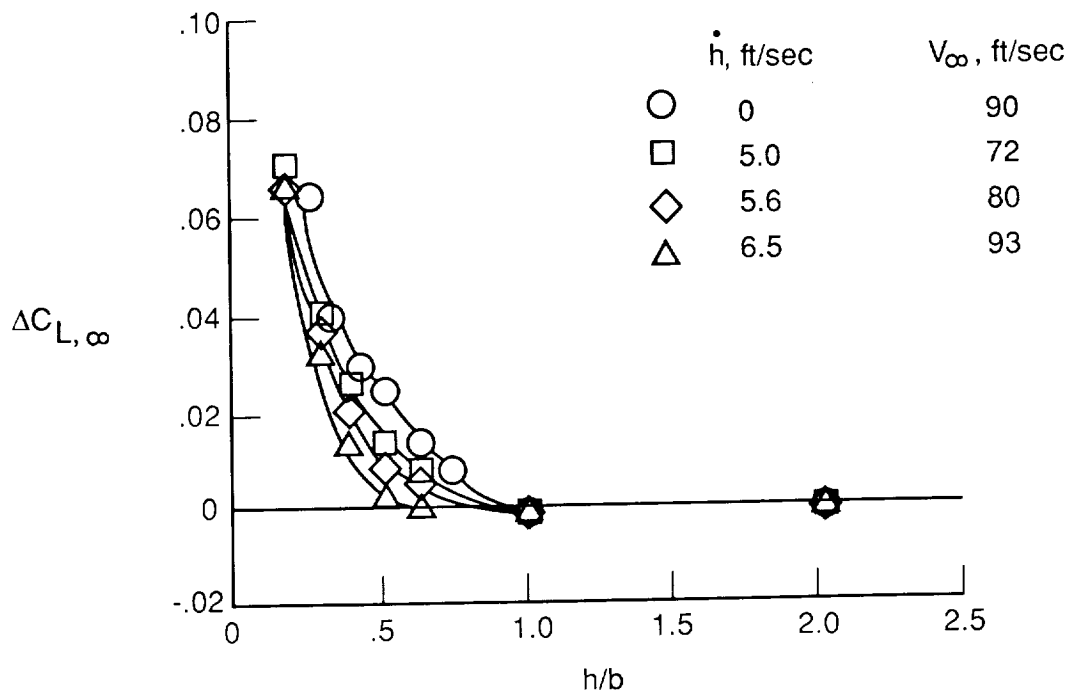
Figure 5. Effect of model height on the lift coefficient of a 60° delta wing at $\alpha = 10°$, NPR = 1.0, and several rates of descent.
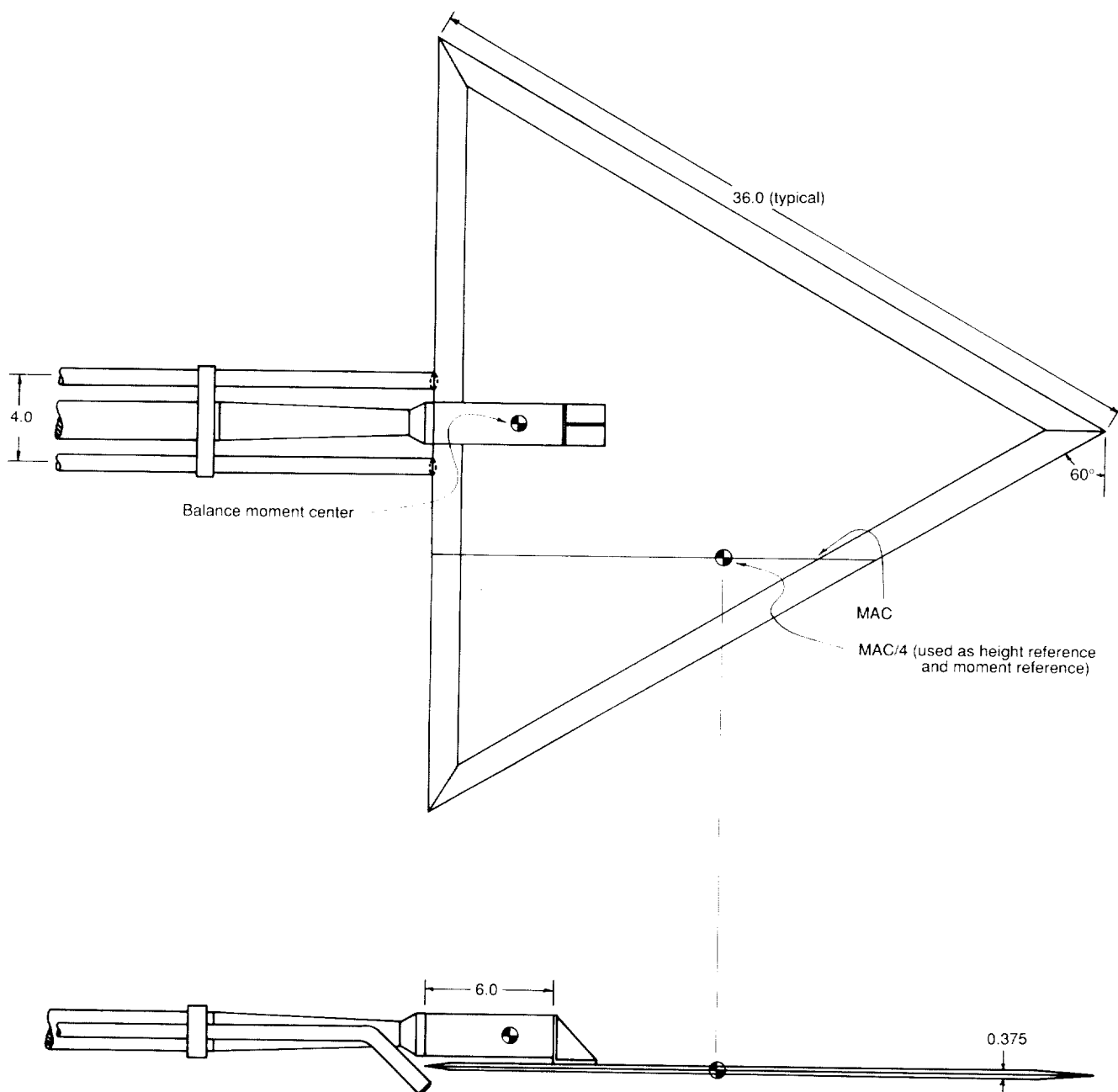
Figure 6. Sketch of the 60° delta wing mounted on the VRF strut. Dimensions are in inches.
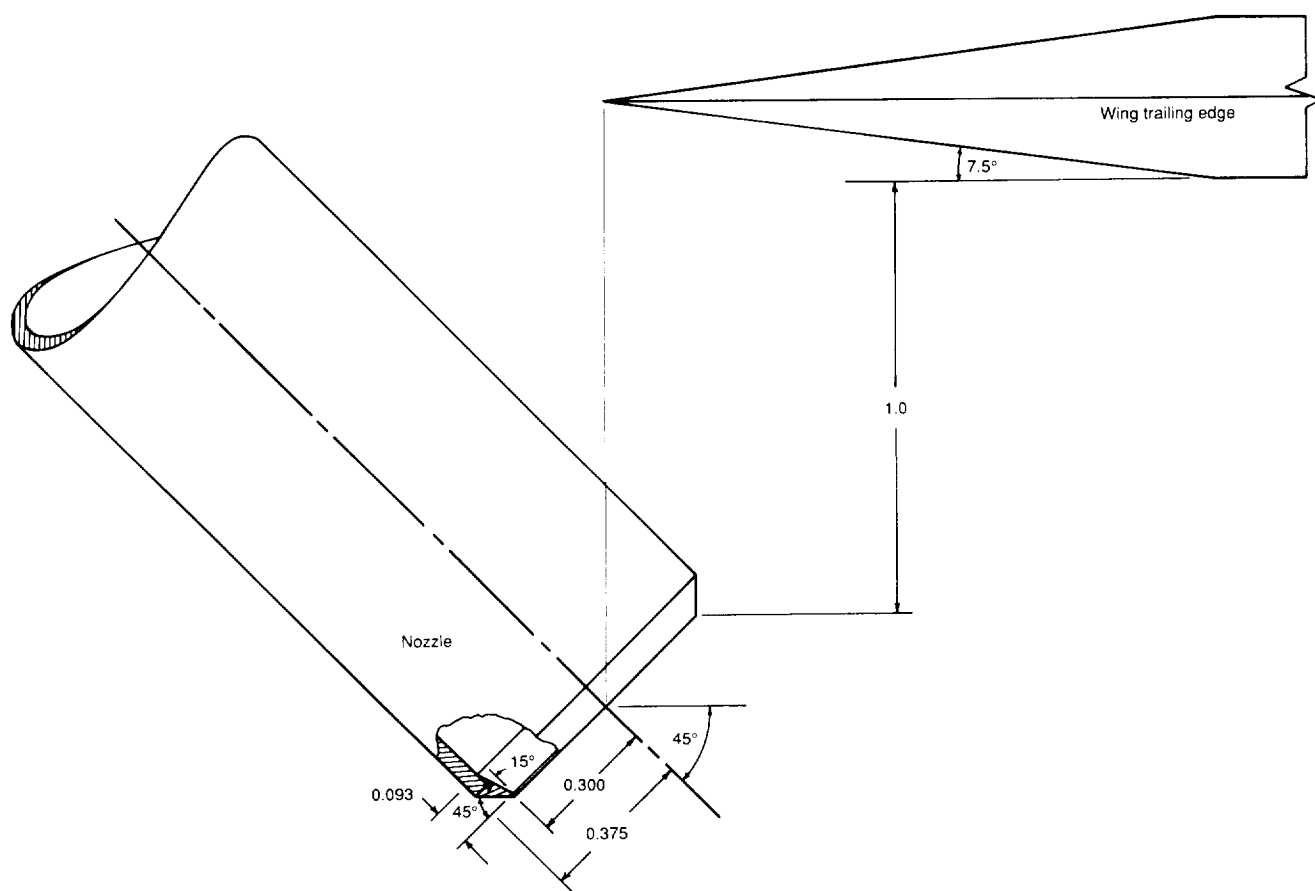
Figure 7. Cross section and relative position of the convergent nozzle used in the 60° delta wing test.
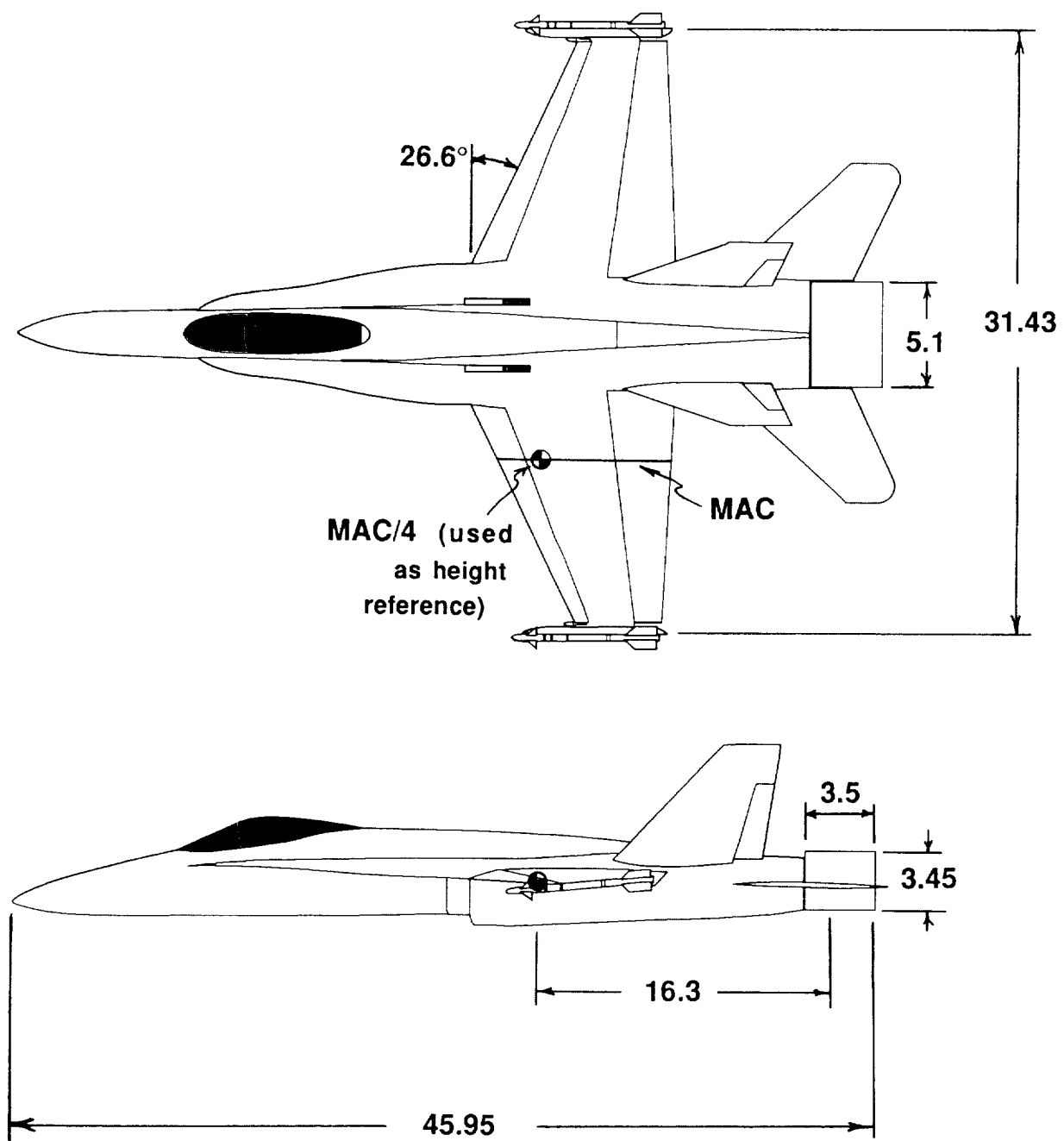
Figure 8. Sketch of the F-18 model tested including some critical dimensions (in inches).
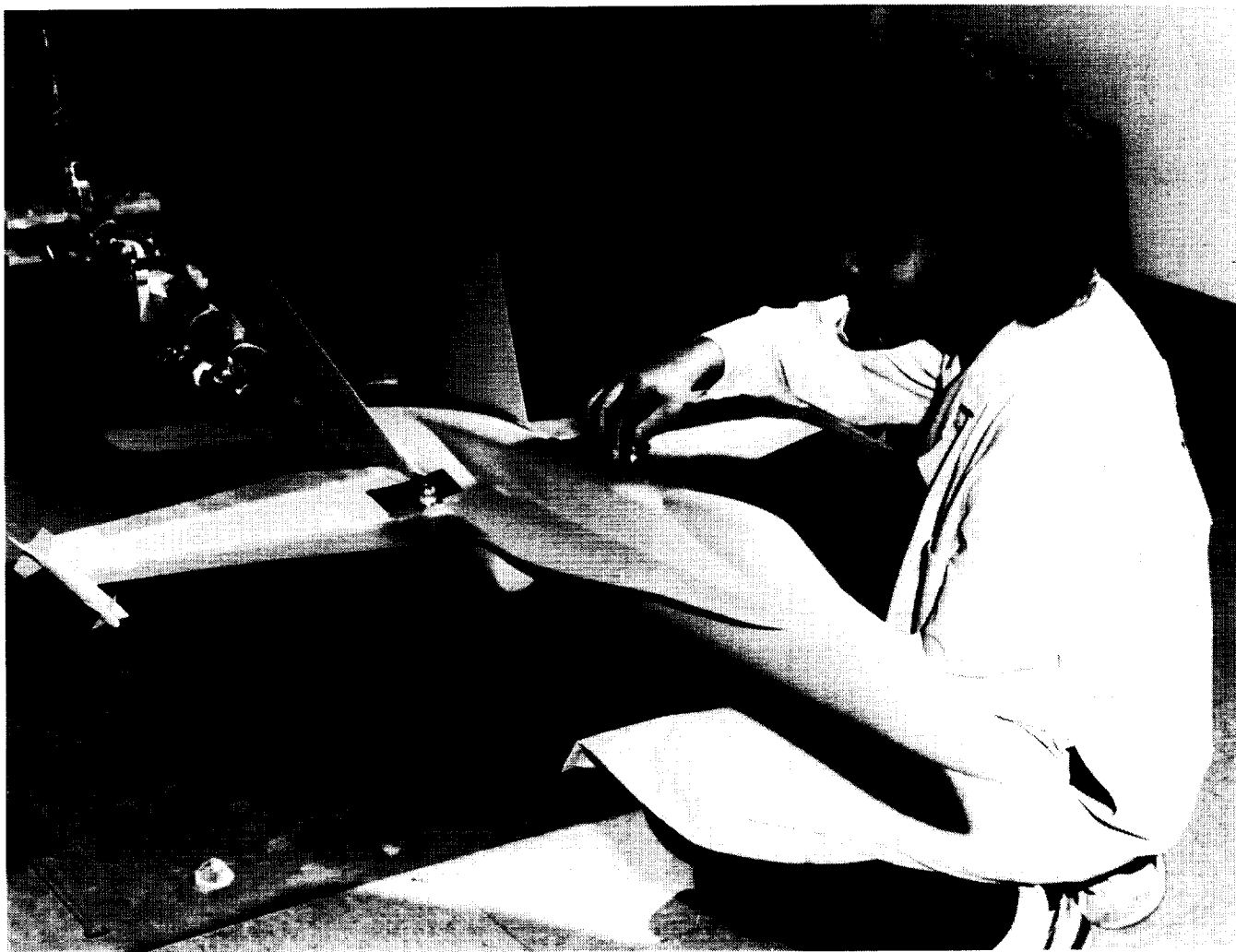
L-86-4528

Figure 9. F-18 model mounted in the VRF.

Sting

Choke basket

45°

Pressure relief valves (4 total)

Honeycomb insert

Air supply lines
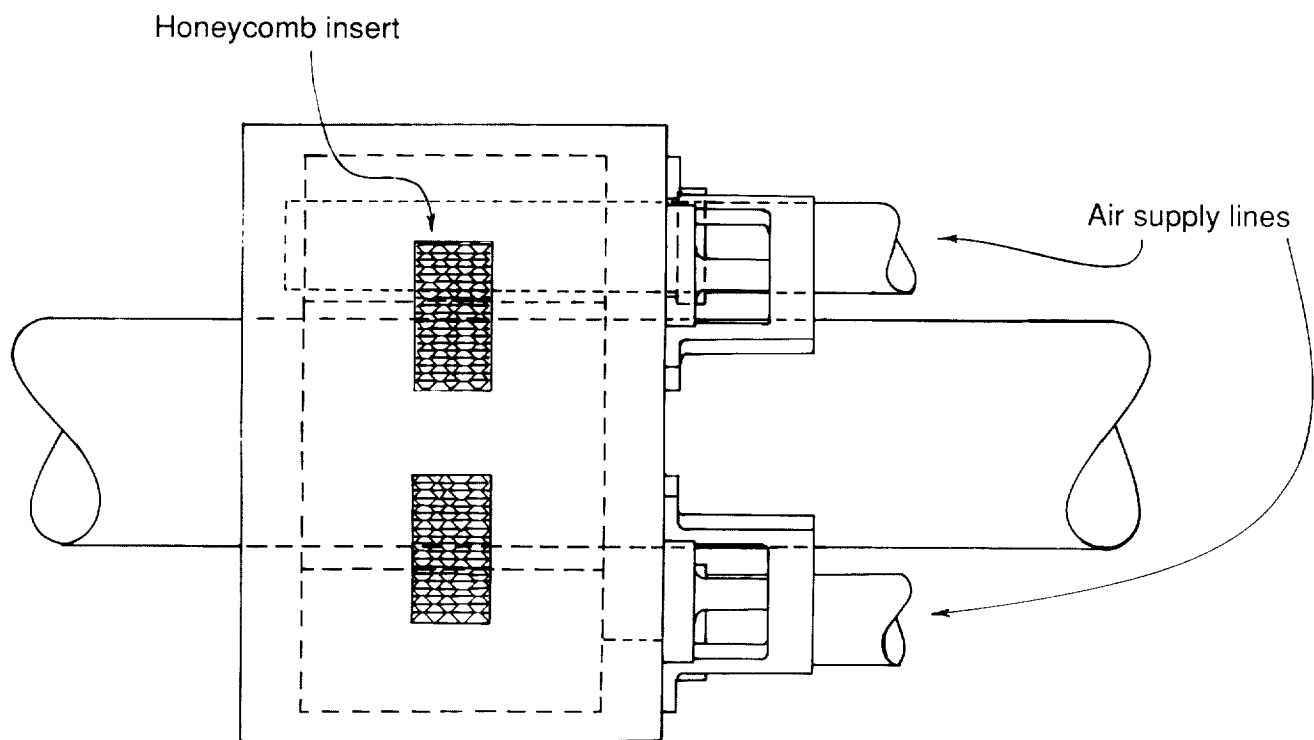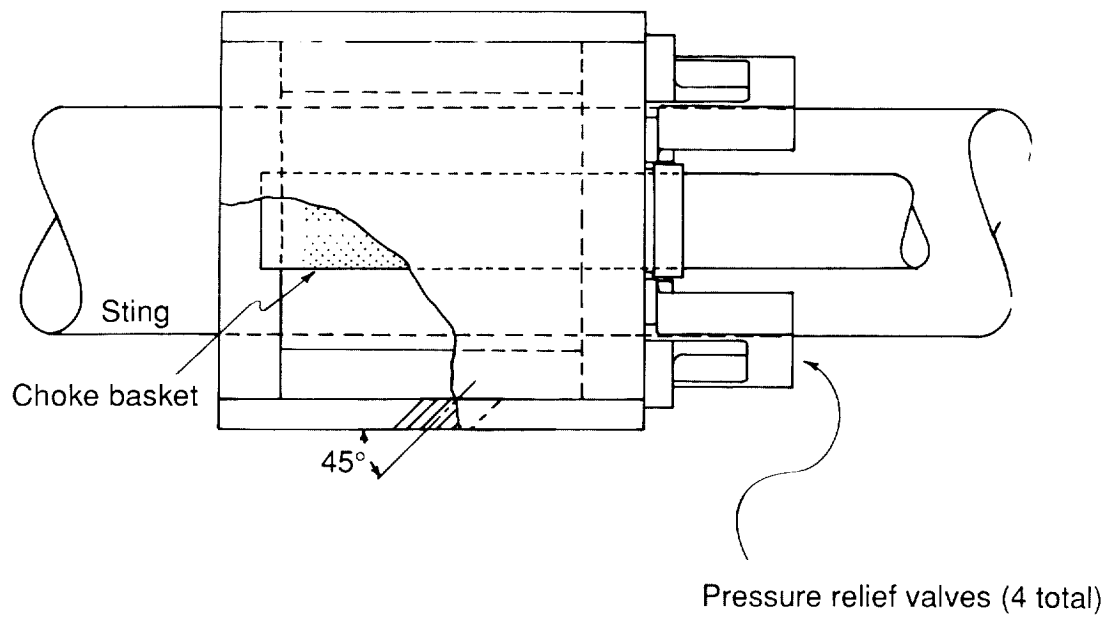
Figure 10. Sketch of the thrust reverser simulator used in the F-18 tests.
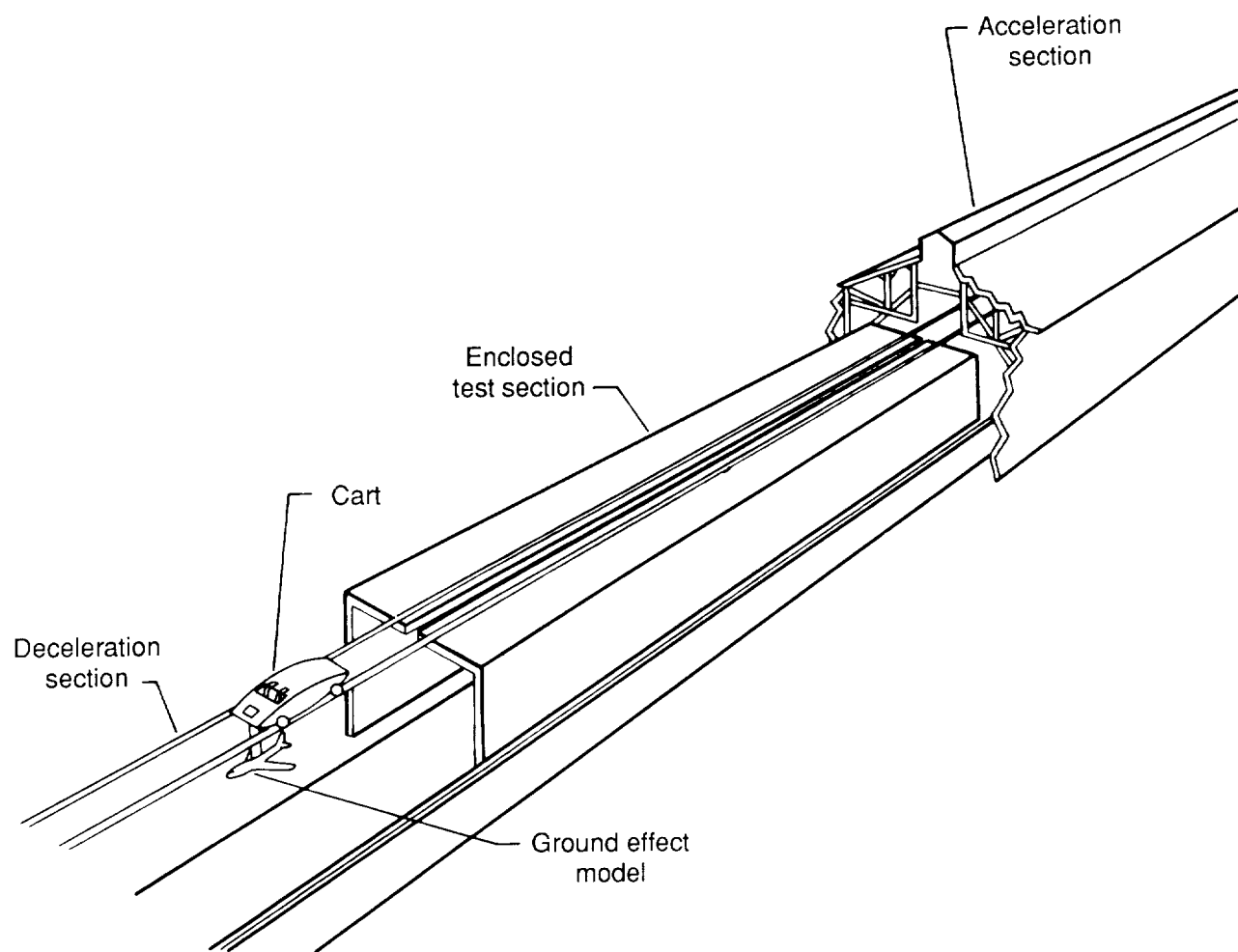
Figure 11. Schematic diagram of the VRF.
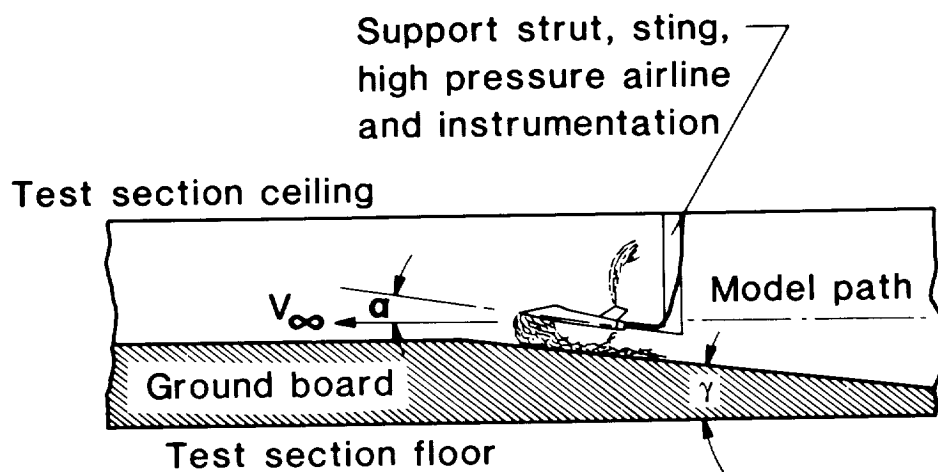
Figure 12. Model passing through the test section in the VRF.
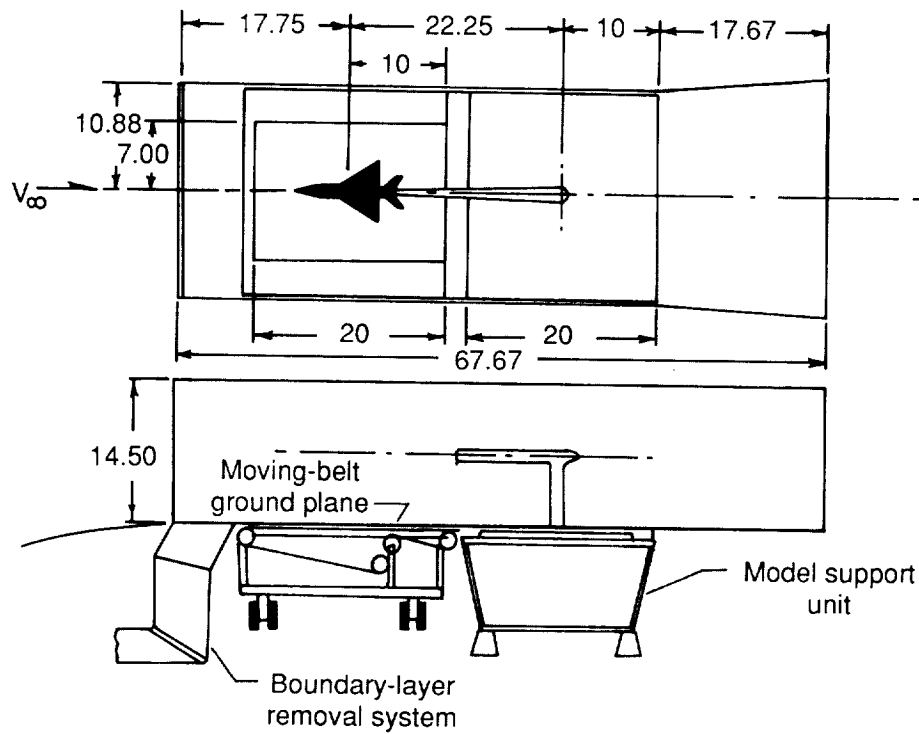
Figure 13. Sketch of the test section in the 14- by 22-Foot Subsonic Tunnel. Dimensions are in feet.
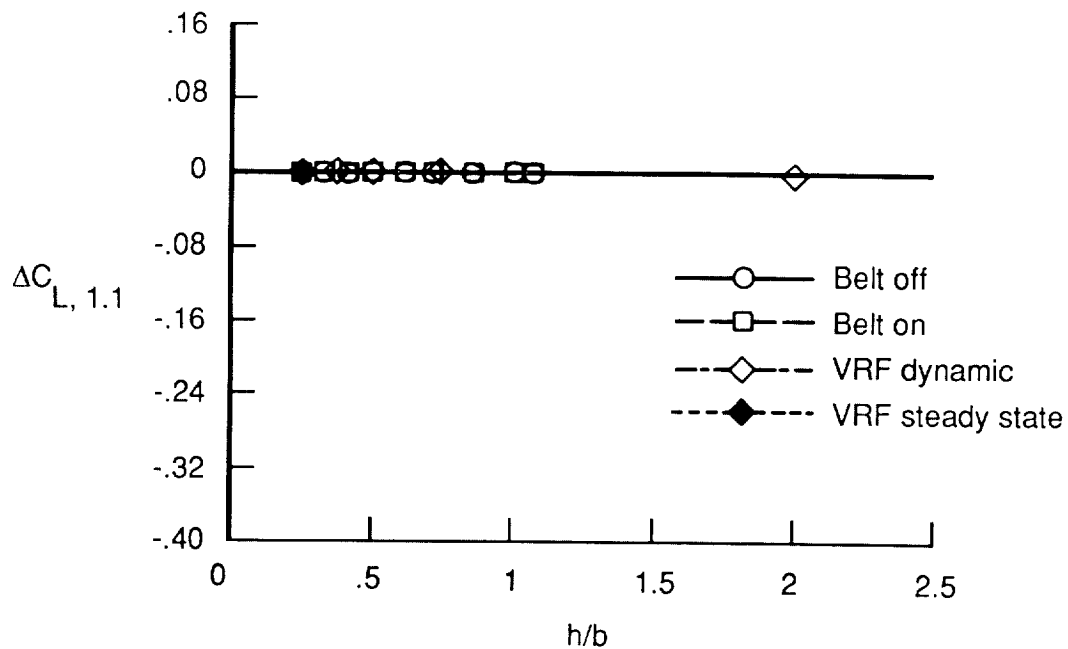
Figure 14. Effect of model height on the lift coefficient of a 60° delta wing at $\alpha = 1.5°$ and NPR = 1.0.
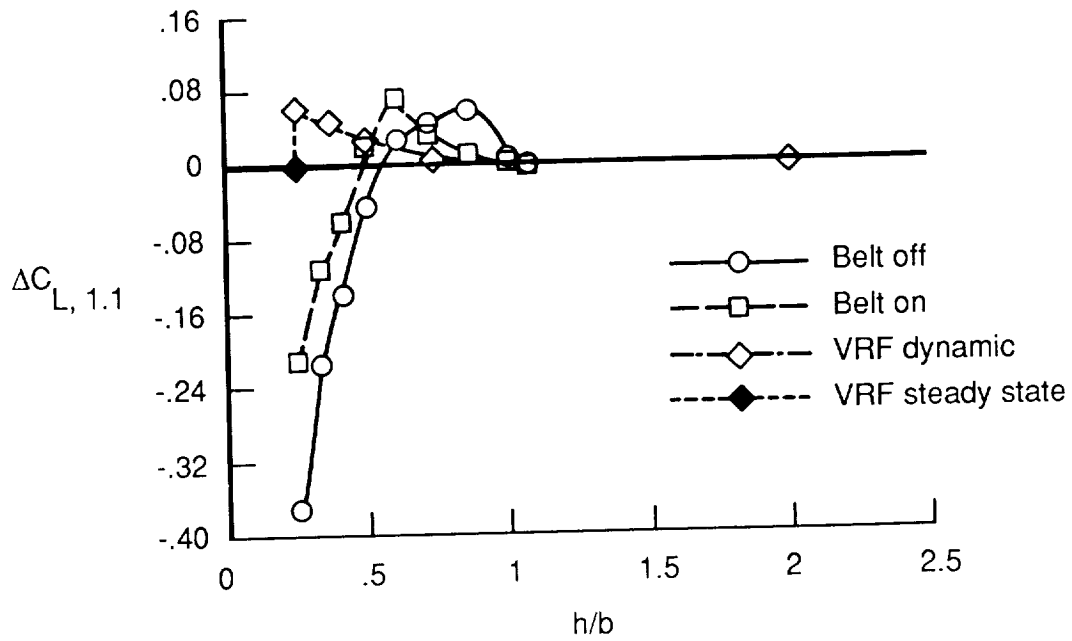
Figure 15. Effect of model height on the lift coefficient of a 60° delta wing at $\alpha = 1.5°$ and NPR = 1.8.
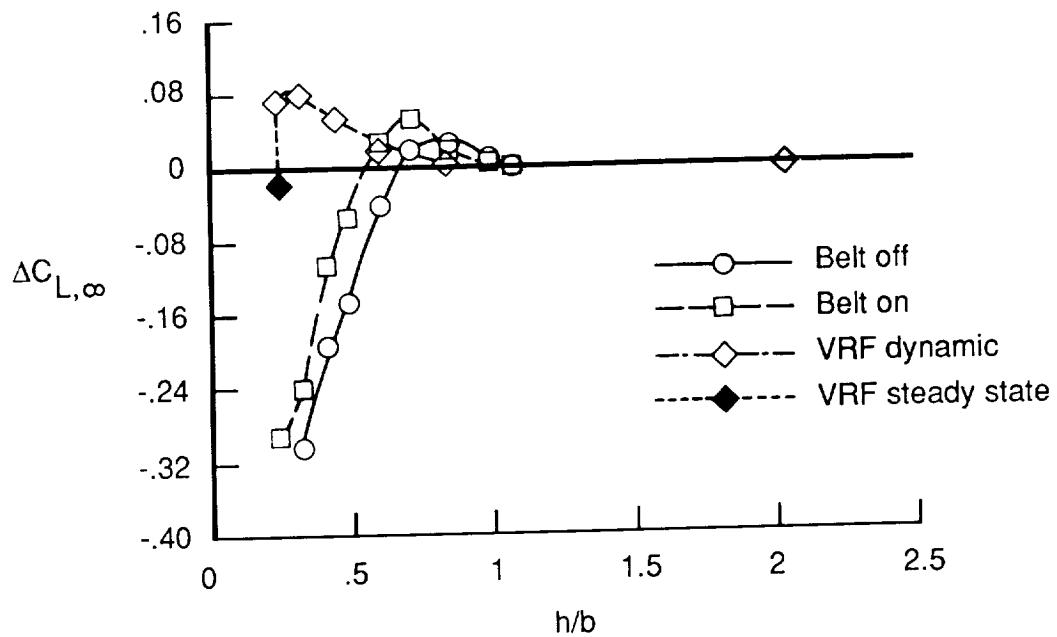
Figure 16. Effect of model height on the lift coefficient of a 60° delta wing at $\alpha = 1.5°$ and NPR = 2.0.
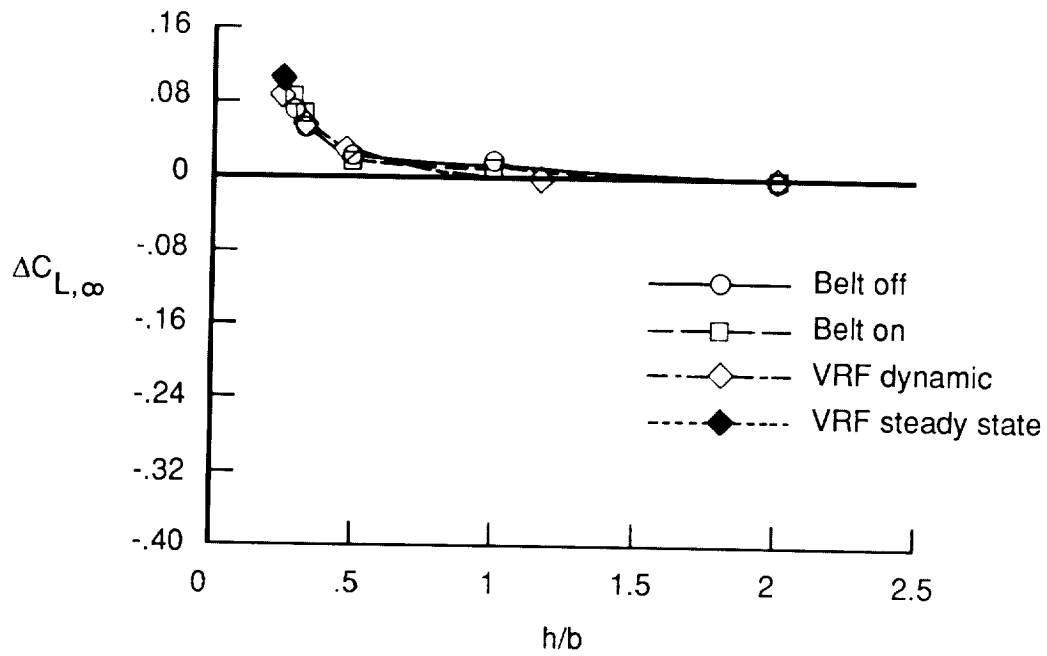
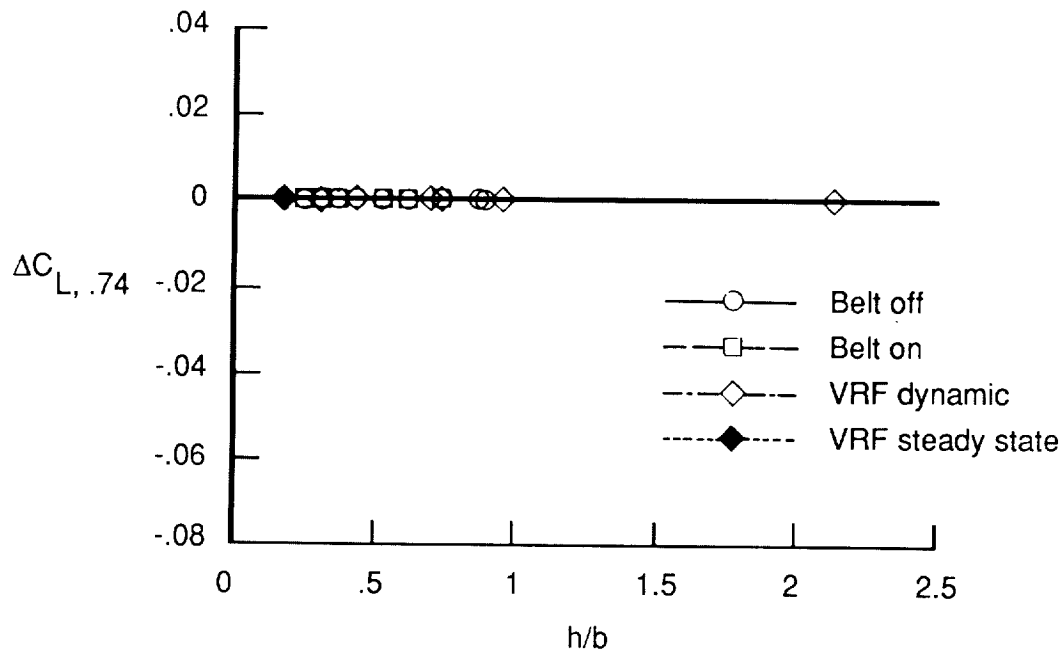Figure 17. Effect of model height on the lift coefficient of a 60° delta wing at $\alpha = 10°$ and NPR = 1.0.
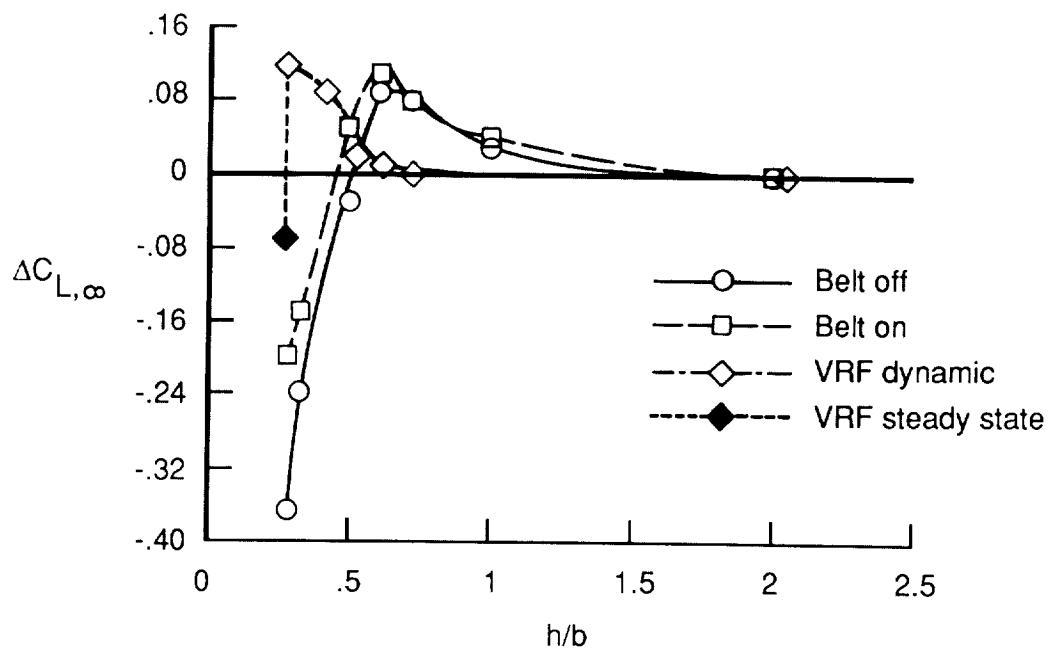
Figure 18. Effect of model height on the lift coefficient of a 60° delta wing at $\alpha = 10°$ and NPR = 1.6.
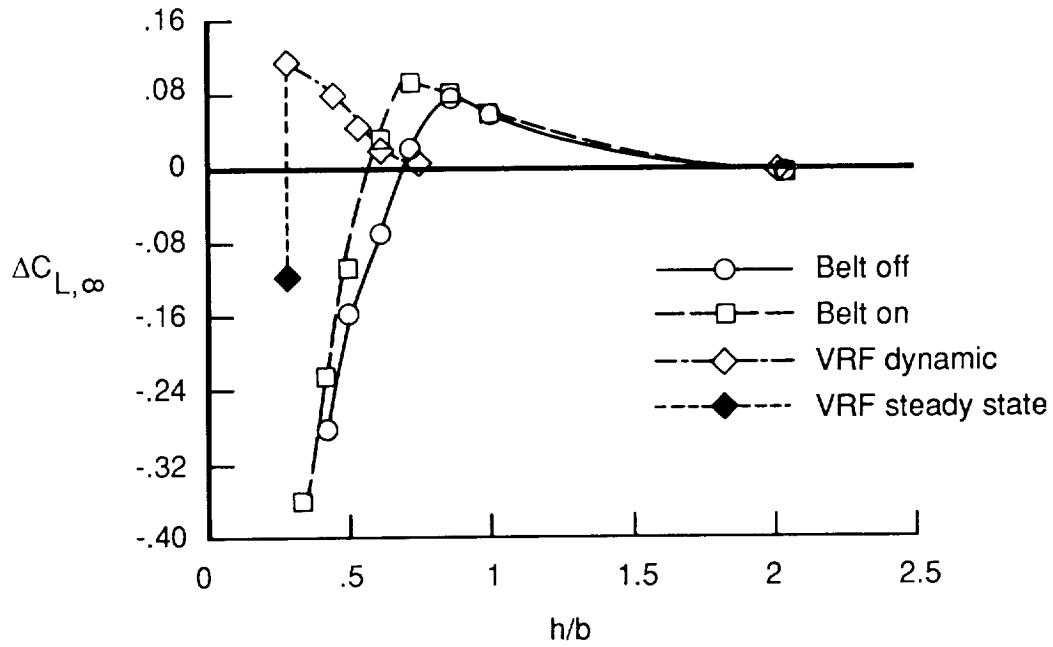
Figure 19. Effect of model height on the lift coefficient of a 60° delta wing at $\alpha = 10°$ and NPR = 2.0.
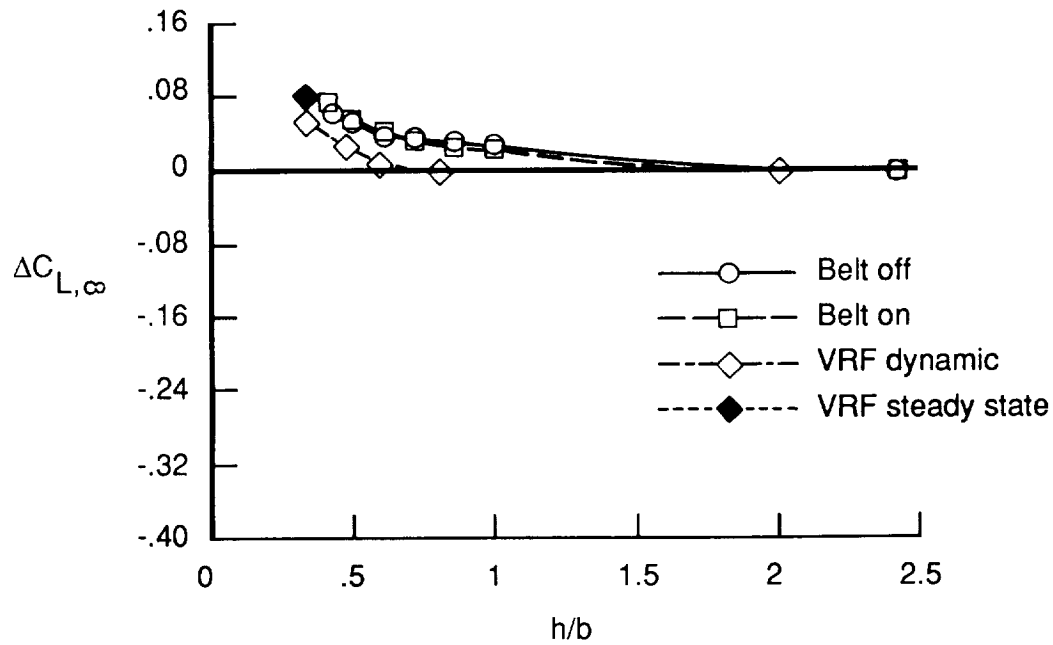
Figure 20. Effect of model height on the lift coefficient of a 60° delta wing at $\alpha = 14°$ and NPR = 1.0.
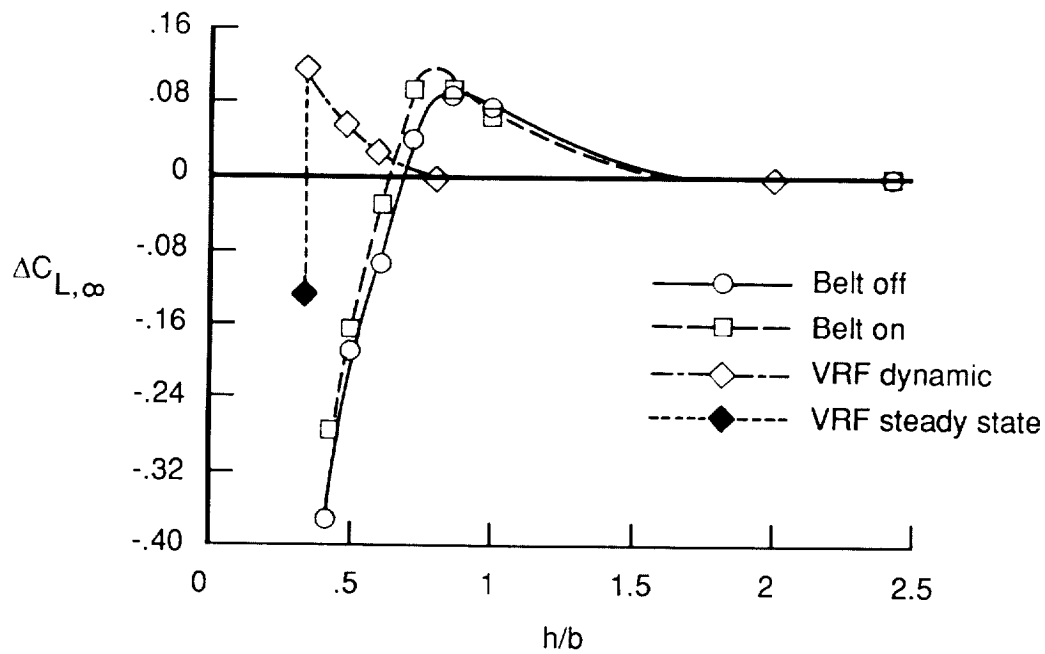
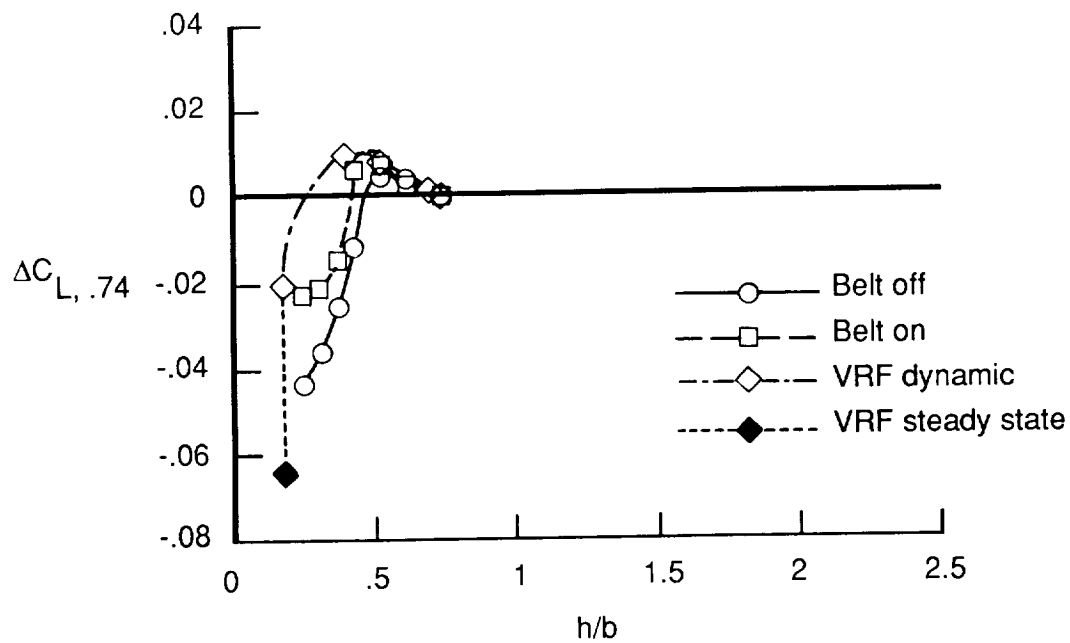Figure 21. Effect of model height on the lift coefficient of a 60° delta wing at $\alpha = 14°$ and NPR = 2.0.

Figure 22. Effect of model height on the lift coefficient of an F-18 model at $\alpha = 1.5°$ and NPR = 1.0. Clean configuration.
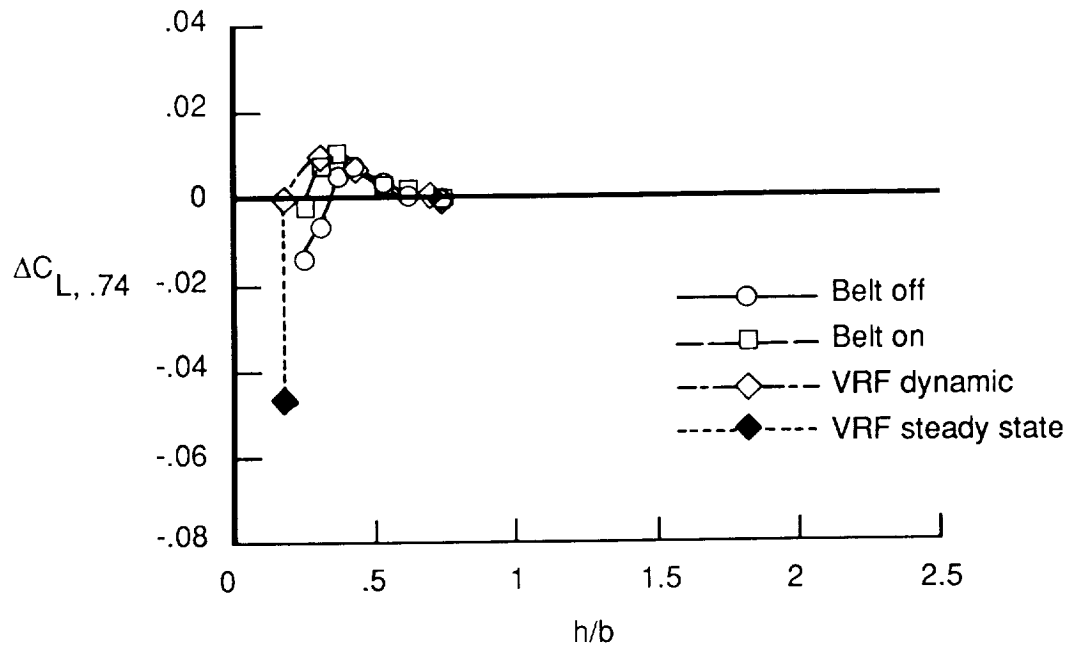
Figure 23. Effect of model height on the lift coefficient of an F-18 model at $\alpha = 1.5°$ and NPR = 1.45. Clean configuration; jets unsplayed.
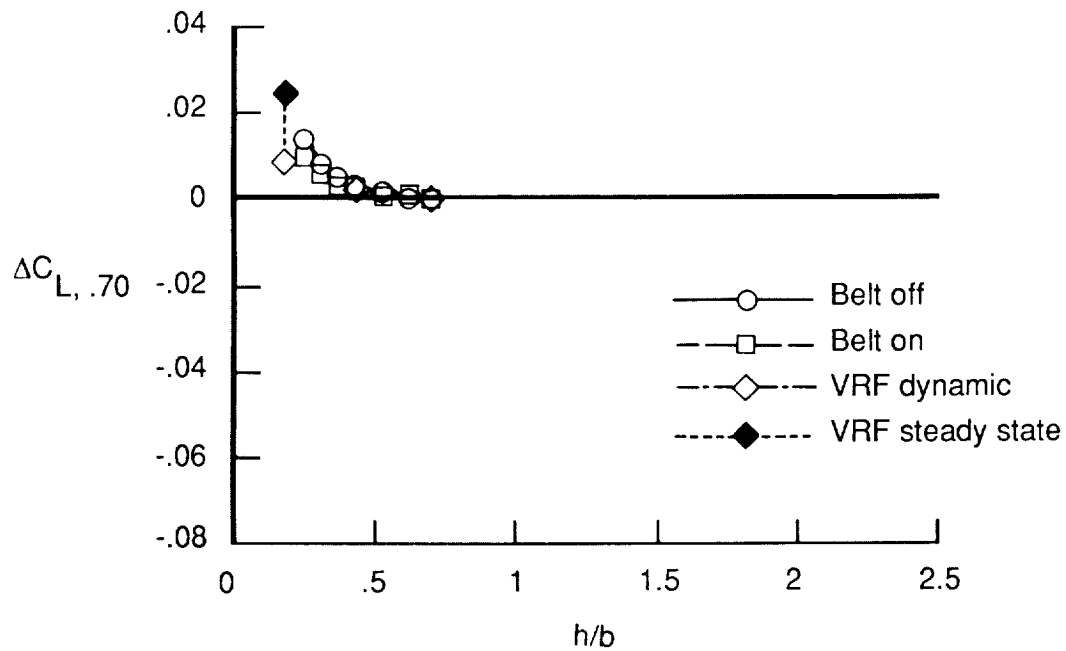

Figure 24. Effect of model height on the lift coefficient of an F-18 model at $\alpha = 1.5°$ and NPR = 1.95. Clean configuration; jets unsplayed.

Figure 25. Effect of model height on the lift coefficient of an F-18 model at $\alpha = 1.5°$ and NPR $= 1.5$. Clean configuration; jets splayed at $40°$.
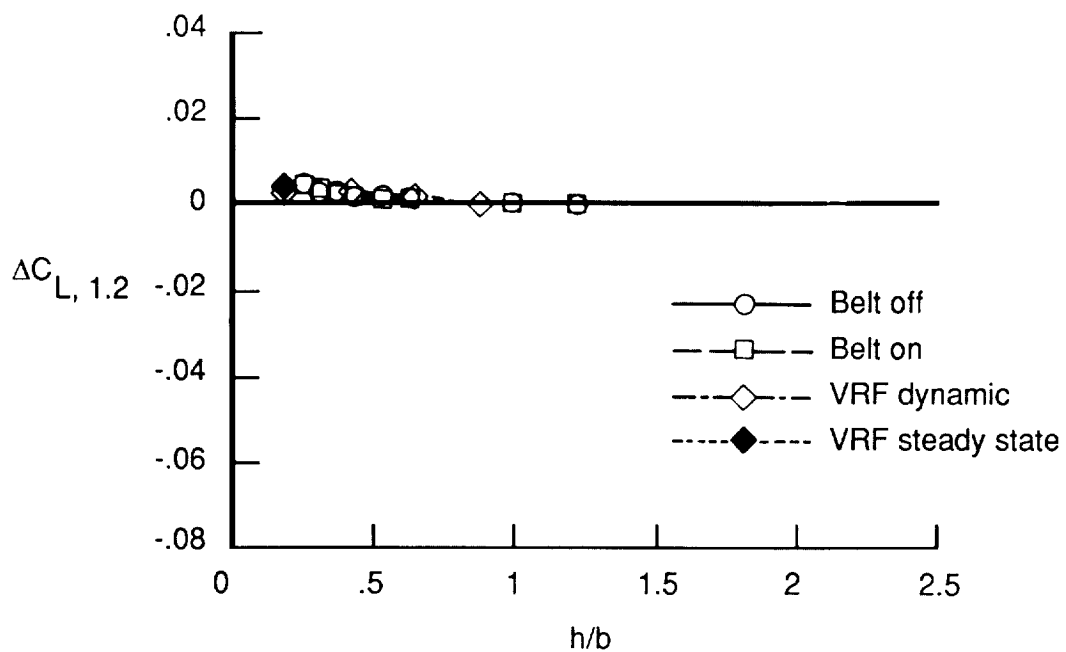

Figure 26. Effect of model height on the lift coefficient of an F-18 model at $\alpha = 1.5°$ and NPR $= 1.0$. High-lift configuration; jets unsplayed.
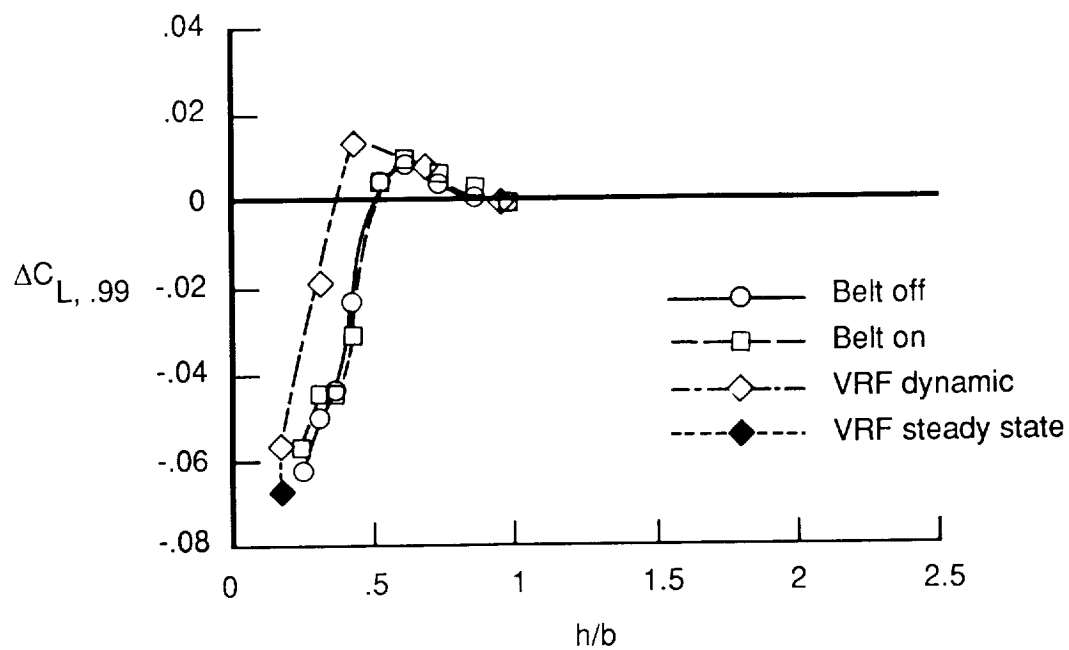
Figure 27. Effect of model height on the lift coefficient of an F-18 model at $\alpha = 1.5°$ and NPR = 2.0. High-lift configuration; jets unsplayed.
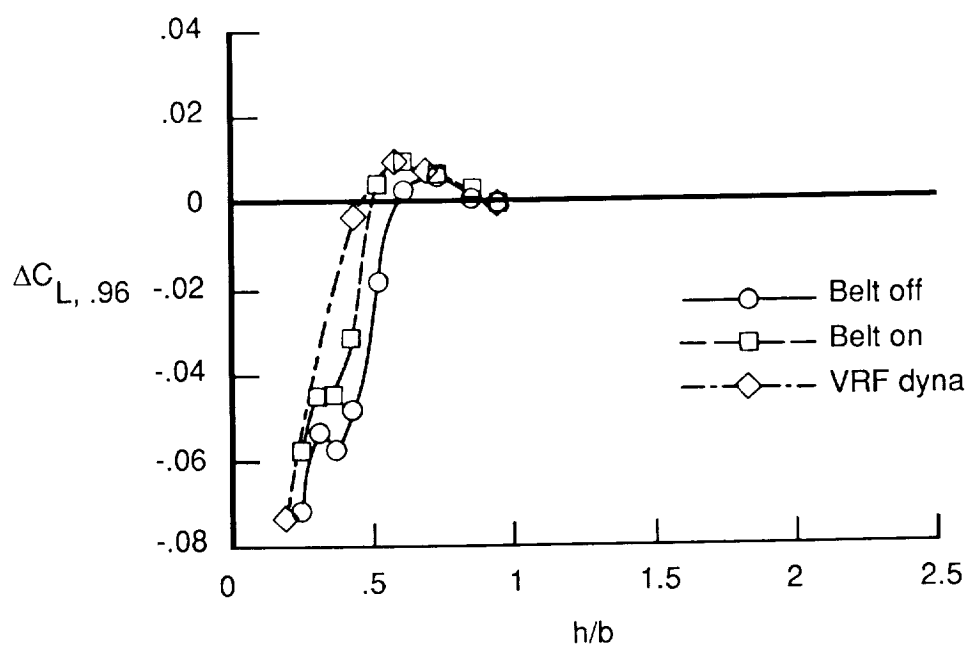

Figure 28. Effect of model height on the lift coefficient of an F-18 model at $\alpha = 1.5°$ and NPR = 2.5. High-lift configuration; jets unsplayed.
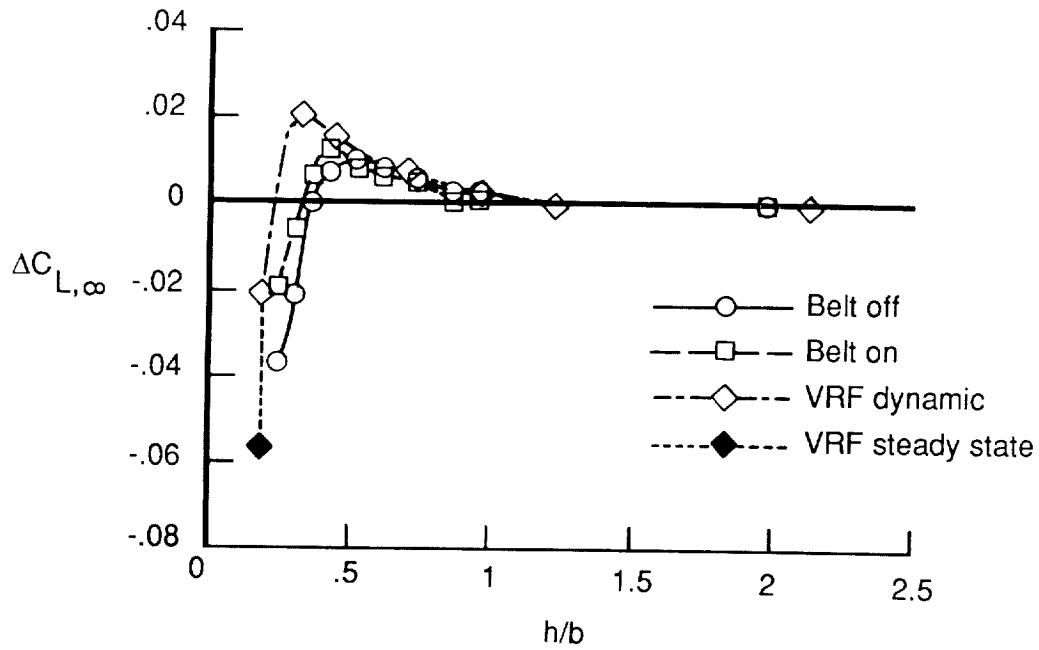
Figure 29. Effect of model height on the lift coefficient of an F-18 model at $\alpha = 8.4°$ and NPR = 1.5. High-lift configuration; jets unsplayed.
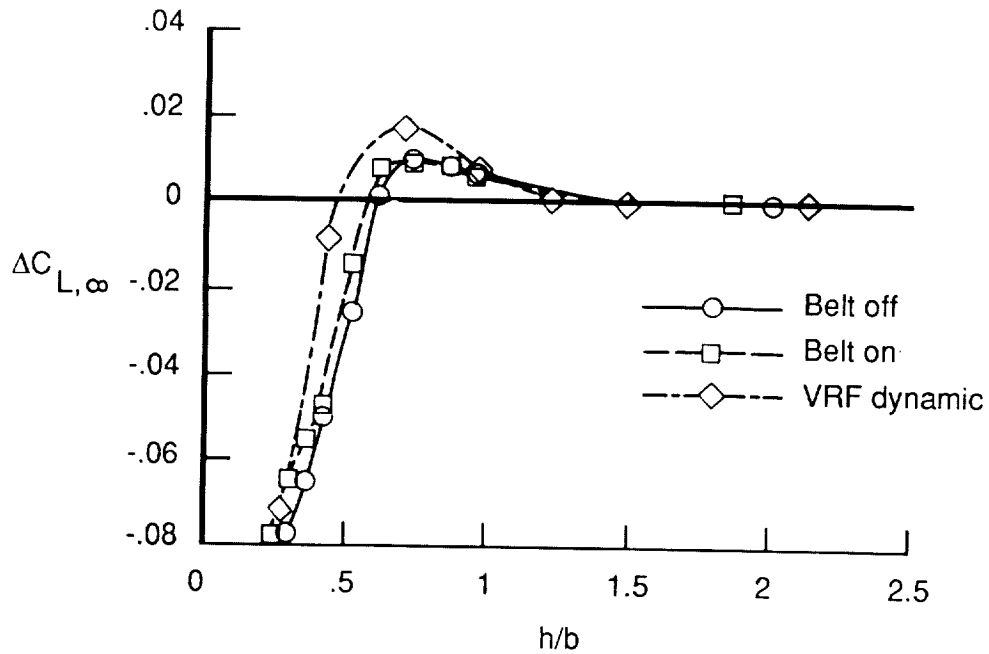

Figure 30. Effect of model height on the lift coefficient of an F-18 model at $\alpha = 8.4°$ and NPR = 2.5. High-lift configuration; jets unsplayed.
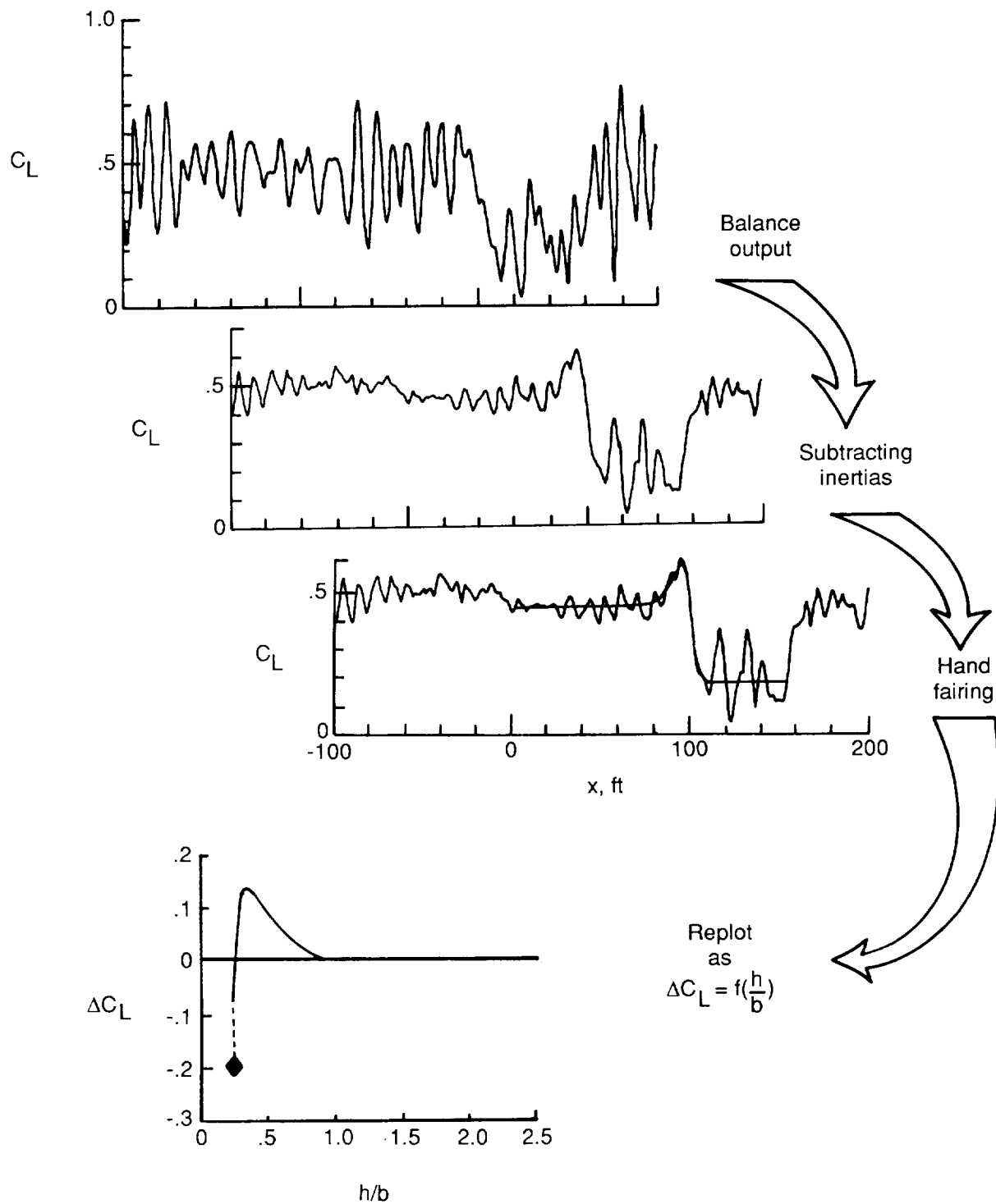
Figure 31. Example of the procedure used to remove the vibrational loads in the VRF data.

Report Documentation Page

1. Report No. NASA TM-4080	2. Government Accession No.	3. Recipient's Catalog No.
4. Title and Subtitle Investigation of a Moving-Model Technique for Measuring Ground Effects		5. Report Date January 1989
		6. Performing Organization Code
7. Author(s) Guy T. Kemmerly and John W. Paulson, Jr.		8. Performing Organization Report No. L-16481
9. Performing Organization Name and Address NASA Langley Research Center Hampton, VA 23665-5225		10. Work Unit No. 505-61-71-02
		11. Contract or Grant No.
12. Sponsoring Agency Name and Address National Aeronautics and Space Administration Washington, DC 20546-0001		13. Type of Report and Period Covered Technical Memorandum
		14. Sponsoring Agency Code

15. Supplementary Notes

16. Abstract

A ground-based testing technique is under development for the measurement of dynamic or time-dependent ground effects which may be present during aircraft approach and landing. The technique utilizes a model moving horizontally over an upwardly inclined ground plane to simulate rate of descent. This method is more representative of flight than conventional wind-tunnel ground-effects testing techniques in which data are obtained at several fixed heights above the ground. Rate of descent simulation is accomplished in the Langley Vortex Research Facility (VRF) by moving a model horizontally over an upwardly inclined ground plane. The model motion over the ramp simulates an approach flight path angle, and the combination of the forward speed of the model and the ramp angle determines the simulated rate of descent. Results were obtained in the VRF for both a 60° delta wing and an F-18 configuration, with and without thrust reversing. The same models and support hardware were also tested in the Langley 14- by 22-Foot Subsonic Tunnel at identical conditions (but, without rate of descent) for comparison.

17. Key Words (Suggested by Authors(s)) Ground effects Thrust reversers F-18 Delta wing Dynamics	18. Distribution Statement Unclassified—Unlimited Subject Category 02	
19. Security Classif.(of this report) Unclassified	20. Security Classif.(of this page) Unclassified	21. No. of Pages 32 · 22. Price A03